12-2017

# Geochemical Controls of Iodine Sorption to Wetland Sediments

Allison C. Sams
*Clemson University*

# GEOCHEMICAL CONTROLS of IODINE SORPTION TO WETLAND SEDIMENTS

---

A Thesis
Presented to
the Graduate School of
Clemson University

---

In Partial Fulfillment
of the Requirements for the Degree
Master of Science
Environmental Engineering and Science

---

by
Allison C. Sams
December 2017

---

Accepted by:
Dr. Brian A. Powell, Committee Co-Chair
Dr. Stephen Moysey, Committee Co-Chair
Dr. Daniel Kaplan

ABSTRACT

Understanding the transformations of iodine during sorption to soils present in redox transition zones is critical for understanding risks from iodine-129 release into the environment. In this work, sorption of iodine to a wetland soil from the Savannah River Site was monitored as a function of time and total iodine concentrations from initially iodide or iodate sources. Batch experiments were performed in order to investigate the effects of organic matter on total iodine sorption and to investigate the rates of iodate and iodide sorption and desorption in a wetland soil. Sorption of iodide was slower than sorption of iodate. Indirect iodine speciation analysis showed that the formation of organoiodine on the surface is important in the sorption process, as aqueous organoiodine is desorbing as iodate continues to sorb to soil. Desorption behavior of initially iodide and iodate showed similar trends, indicating that iodine transforms into the same species regardless of starting speciation (i.e. iodide or iodate). Most likely, the iodine is transforming via a surface-mediated process to organoiodine; due to the indirect methods of determining iodine speciation, the desorbing iodine species is uncertain, but it is most likely organoiodine. A numerical solution was created to approximate the desorption behavior observed in experiments starting with both iodide and iodate and a single set of forward and reverse rate constants was required to describe all of the data. Multiple rate laws were examined to fit both the sorption and desorption data but none followed standard laws with integer reaction stoichiometries.

ACKNOWLEDGMENTS

I would like to thank my co-advisors, Dr. Brian Powell and Dr. Stephen Moysey, and my other committee member, Dr. Daniel Kaplan for all of their assistance and expertise. Additionally, thank you to all of the members of Dr. Powell's and Dr. Moysey's research groups for offering their insights and for aiding in the lab, especially Yu Xie, Rebecca Dozier, and J. Britton Hundley Jr. Thank you, Dr. Mine Dogan, for creating the numerical kinetic desorption model in MATLAB and for assistance with all of the accompanying writing. I would also like to thank Mahmut Selim for technical assistance and Dr. Ayman Seliman for additional help in the lab and for providing the N-methyldi-n-octylamine (MDOA) resin.

This research was supported by the U.S. Department of Energy Office of Science, Office of Basic Energy Sciences and Office of Biological and Environmental Research under Award Number DE-SC-00012530

TABLE OF CONTENTS

Page

Table of Contents (Continued)

Page

LIST OF FIGURES

Figure Page

LIST OF FIGURES (CONTINUED)

FIGURE PAGE

List of Figures (Continued)

Figure Page

List of Figures (Continued)

Figure Page

LIST OF TABLES

Table Page

List of Tables (Continued)

Table Page

List of Tables (Continued)

Table Page

# 1. INTRODUCTION

## 1.1 BACKGROUND

Iodine-129 ($^{129}$I) is one of the top three risk drivers in radiological waste disposal. Anthropogenic $^{129}$I is generated mainly through fuel reprocessing, with a small portion attributed to atmospheric bomb testing. Iodine-129 is a concern due to its long half-life (almost 16 million years), high inventory in radiological waste disposal, high toxicity, high mobility in environmental systems, and biophilic nature (Chang *et al.,* 2014). In the human body, 90% of the iodine is in the thyroid where it accumulates as triiodothyronine and thyroxine (Kaplan *et al.,* 2011, Zhang *et al.,* 2011).

The Savannah River Site (SRS) is a Department of Energy laboratory located in Aiken, South Carolina. From 1955 to 1988, the SRS generated radionuclides primarily for the production of nuclear weapons (Otosaka *et al.,* 2011). Seepage basins in the SRS F-area were used to dispose of approximately $7 \times 10^6$ m$^3$ of acidic waste comprised of dozens of radionuclides (including $^{129}$I, tritium, plutonium-239, and more), metals (including mercury and lead), and high concentrations of nitric acid that resulted in a source term with an average pH of 2.9 (SRNS, 2010, Looney *et al.,* 1987). In 1988, the usage of the F-area seepage basins were terminated. The seepage basins were remediated by removing approximately a 0.6-meter-depth of sediment, mixing in limestone and blast furnace slag, refilling it with back fill soil, and then capping it with a low permeability RCRA clay cap (Denham and Vangelas, 2008, Kaplan *et al.,* 2011). This combination of remediation approaches successfully reduced the mobility of plutonium, technetium, and

uranium. However, as pH increased the concentration of aqueous iodine-129 increased (Kaplan *et al.,* 2011).

Several of the highest concentrations of $^{129}I$ in subsurface pore waters at legacy weapons sites in the United States have been measured at the SRS in the F-area Seepage Basin. Some wells in the F-area at SRS have concentrations as high as 10 to 100 pCi/L, two orders of magnitude higher than the US-EPA maximum contaminant level in groundwater of 1 pCi/L (Federal Register, 2000). The highest concentration at SRS was reported in 2009 at 1060 pCi/L, down-gradient of the largest waste disposal basin. The radioiodine concentration continues to increase in some wells in the F-area at the SRS, which is associated with increasing pH at the seepage basins, the source term (Kaplan *et al.,* 2011). The $^{129}I$ concentration in well FSB-95DR increased from 1993 to 2010. Well FSB-110D has undergone a decrease in $^{129}I$ since 1999, and the $^{129}I$ concentrations in other wells in the F-area have been relatively consistent (Kaplan *et al.,* 2011, Figure 1).

Wetland soils have distinctive characteristics in comparison to upland soils. The most important one for this project is the accumulation of organic matter, which can serve as a source of electron donors and facilitate the transformation of iodide or iodate to organoiodine compounds (Schwehr *et al.,* 2009, Schwehr and Santschi, 2003). The organic matter content varies between different wetland soils. Wetland soils also have increased capability to reduce inorganic electron acceptors, which results in accumulation of reduced species in the soil. There are many parameters that affect the exchange of dissolved species including 1) the concentration of the dissolved compound in the groundwater 2) soil type, 3) other physicochemical parameters such as pH, cation

exchange capacity, organic matter content, oxidation-reduction potential, and bulk density, and 4) the kinetics of the biogeochemical processes between soil and groundwater.

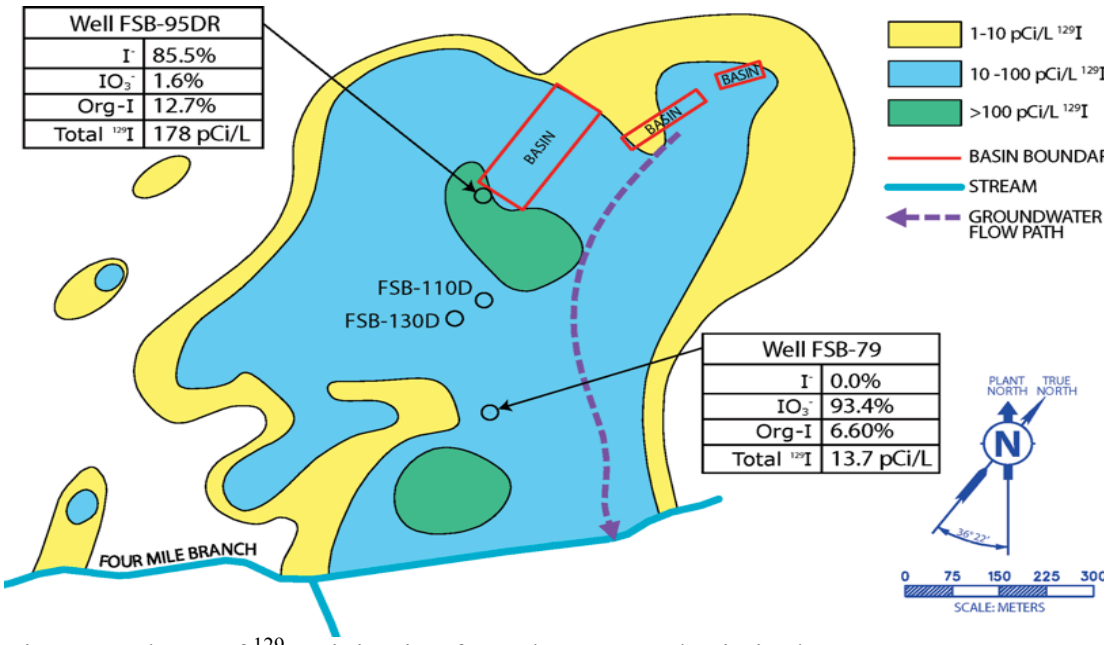


Figure 1. Plume of $^{129}I$ originating from the seepage basin in the SRS F-area. Reprinted with permission from Kaplan *et al.,* 2011. Copyright 2011 American Chemical Society.

Iodine in soils can be complexed with organic matter via covalent bonding to aromatic carbon or phenolic moieties in soil organic matter (Zhang *et al.,* 2011 and references within). Iodination of aromatic moieties can be accelerated or obstructed by adjacent functional groups. The fulvic acid fraction of organic matter tends to have higher reactivity with iodine due to the lower molecular weight of the organic compounds (Warner *et al.,* 2000). Iodine bound to organic matter with higher molecular weight, such as humic acid, is less mobile than iodine bound to the lower molecular weight fulvic acid fraction (Zhang *et al.,* 2011).

Despite generally weak sorption of iodide as a monovalent anion, there has been significant sorption of iodine in the SRS subsurface. Geochemical controls on iodine sorption have been studied as result. Relatively high sorption has been attributed to the high zero-points-of-charge and clay soil containing iron, which facilitates ion interactions between iodide and the surface of the soil (Kaplan *et al.,* 2000, Hu *et al.,* 2005). It has been found in several studies that pH and iodine concentration significantly affect sorption. At ambient concentrations, iodide tends to be more immobilized than at elevated concentrations of iodide (Zhang *et al.,* 2011, Emerson *et al.,* 2014). Distribution coefficients ($K_d$) increased with decreased concentrations of iodide and iodate in SRS upland and SRS wetland soils (Emerson *et al.,* 2014). This is contrary to the definition of the $K_d$ construct, which states that the partitioning of a solute (radionuclide) between the aqueous and solid phases remains constant with solute concentrations.

Iodine in soils may exist in many forms under environmental conditions with the three major species as: iodide ($I^-$), iodate ($IO_3^-$), or organoiodine (org-I) for both $^{127}I$ and $^{129}I$. Less common species are hypoiodous acid (HOI) and molecular iodine ($I_2$) (Chang *et al.,* 2014). The dominant species in freshwater and estuarine environments is iodide (Hou *et al.,* 2009). Iodine-129 is primarily disposed of at SRS in the form of iodide ($I^-$), which slowly converts to iodate and organoiodine along 0.7 km of subsurface in the F-area (Chang *et al.,* 2014). The speciation of iodine in soils is dependent mainly on the geochemistry of the system where variances in oxidation-reduction potential, pH, dissolved organic carbon, and microbial activity can promote transformation between iodine species (Chang *et al.,* 2014, Zhang *et al.,* 2011, Li *et al.,* 2013).

Knowing rates of iodine sorption and desorption could aid in the understanding of iodine transport in the environment. However, in many cases the rate laws must be independently determined as iodine sorption to soils varies depending on the speciation. Typically, iodide sorbs measurably less than iodate and organoiodine (Chang *et al.,* 2014). Humic acid in soil is able to reduce iodate and oxidize iodide, binding the species that is formed (Bowley *et al.,* 2016). Aqueous iodine binds with humic substances in a two-step manner, with an initial rapid complexation and then a slower uptake by humic substances (Warner *et al*., 2000). Iodide and iodate in soils is predominantly converted to organoiodine via enzymatic transformation by bacteria (Suresh *et al.,* 2008). Thyroxine (the iodine-containing hormone in the human thyroid) and protein iodination follows Michaelis-Menten enzyme kinetics (Huber *et al.,* 1989, Pommier *et al.,* 2005). Enzymes in bacteria cause iodination of natural organic matter, therefore it is possible that bacterial enzymes in soil follow the same kinetics as enzymes in the human thyroid (Amachi *et al.,* 2005).

## 1.2 KNOWLEDGE GAPS AND OBJECTIVES

Organoiodine formation from iodide and iodate is common in soils. Iodine is expected to bind to aromatic carbon in soil organic matter, specifically phenolic type structures in humic acid (Xu *et al.,* 2013). Also unknown is how the initial iodine speciation affects iodine sorption to soils and organic matter. At artificially elevated iodine concentrations, Emerson *et al.* (2014) shows the distribution coefficient ($K_d$) varies with iodine concentration. However, this is not the definition of a $K_d$ because there

should be no variability of $K_d$ with sorbate concentrations. Some general information about iodine sorption rates is available. It has been reported that iodine binding with humic acid follows a series of reversible first-order reactions (Bowley *et al.,* 2016). However, this study ignores the soil and the remainder of the organic matter. There are several limitations of other studies on kinetic iodine sorption including the time resolution of the kinetic experiment is on the order of days as opposed to hours, and some are conducted at artificially elevated iodine concentrations (Schwehr *et al.,* 2009). The detailed kinetics of sorption and desorption of iodine when iodide and iodate are added to a soil are unknown. Understanding the kinetics and geochemical controls of iodine sorption is fundamental to predicting the transport of iodine in the subsurface.

This thesis has three primary objectives to gain an understanding of the behavior of iodine in the presence of a wetland soil from the F-area at SRS. The deliverables from these objectives will include sorption distribution coefficients and rate expressions describing iodine sorption versus time and iodine total concentrations. The first objective is to determine the relative rates at which iodide and iodate sorb and desorb in a high organic matter soil. The second objective is to determine the distribution between organic and inorganic iodine species after allowing aqueous iodine to equilibrate in a wetland soil. The third objective is to create a conceptual model of the kinetic processes occurring in a system starting with aqueous iodine (as iodide or iodate) and a high organic matter soil.

## 2. MATERIALS AND METHODS

All water used in experiments was Distilled Deionized (DDI) water with a resistivity greater than 18.2 MΩ.cm and 2 ppb or less of total organic carbon. All plastic centrifuge tubes and plastic bottles used for making and storing working solutions and samples were first soaked in 0.01 M sodium chloride (NaCl) in DDI water solution for sixteen to twenty-four hours, rinsed with DDI water, and allowed to completely air dry. The intent of soaking all of the tubes before using them was to minimize sorption of iodine to the vial walls, to prevent artifacts from colloidal contamination, and to leach residual organic plasticizers from the plastic tubes.

### 2.1 SRS WETLAND SOIL CHARACTERIZATION

Organic carbon content on the SRS wetland soil was measured by loss-on-ignition, based on the standard methods in Sparks *et al.,* 1996. Inorganic dehydroxylation was assumed to be negligible in the SRS wetland soil, therefore loss-on-ignition percent was assumed to equal organic matter percent. In order to determine the concentration of extractable iodine native to the SRS wetland soil, 0.5 g of the soil was weighed out into a pre-soaked 15 mL centrifuge tube. Ten milliliters of 0.01 M sodium hydroxide (NaOH) was added to the soil. It was anticipated that the NaOH solution would extract the exchangeable iodine and the readily extractable organic-bound iodine. Triplicate samples were made. The soil was allowed to equilibrate in the NaOH solution for thirteen days. The samples were then centrifuged at 8000 rpm for 30 minutes. Supernatant was removed and saved for analysis by inductively coupled plasma mass spectrometry (ICP-MS) on a

Thermo XSeries II ICP−MS. Even after centrifuging, supernatant was a translucent brown-orange, most likely due to dissolved soil organic matter. Due to the visibly high amount of aqueous organic matter in the samples, they were run with ethylenediaminetetraacetic acid (EDTA) on the ICP-MS to protect the instrument.

## 2.2 BATCH SORPTION EXPERIMENT

The first set of experiments was performed using mixtures of two different soils: a sandy loam soil from the SRS West Borrow pit which is referred to as the "SRS upland soil" and a wetland sediment; the wetland sediment was collected on August 15, 2016 by Dan Kaplan (Savannah River National Laboratory, Aiken, SC) from 0 – 10 cm depth from the surface near Tim's Branch creek, and it is referred to as the "SRS wetland soil." Subsamples of both soils were sieved to 2 mm and air-dried separately before use in experiments. Batch sorption experiments were performed in 15 mL polypropylene centrifuge tubes containing 0.01 M NaCl and 50 g/L of upland or wetland sediments and a total volume of 10 mL. The 50 g/L of soil was added with different ratios of SRS wetland to SRS upland soil (5/95, 10/90, 20/80, 50/50, and 75/25) in order to vary the amount of organic matter in each batch test. Stable sodium iodide (NaI) was spiked into each sample to achieve a concentration of approximately 5000 ppb. Samples were taken after three days, fourteen days, and eight weeks after spiking the samples. The pH was adjusted to $5.0 \pm 0.05$ at the beginning of the batch experiment, to better match the natural pH of the soil; after the samples were made, the pH was measured but not adjusted during the length of the experiment. The samples were placed on a mixer for …

At each sampling event, the batch samples were removed from the mixer, and a homogenous 1.5 mL aliquot from each suspension was removed with a pipette. Aliquots were transferred into 1.8 mL centrifuge tubes and centrifuged at 8000 RPM for 20 minutes to separate suspended solids. Aliquots of 1.0 mL of the supernatant were placed into new 15 mL polypropylene centrifuge tubes, and diluted with an additional 4.0 mL of DDI water, and saved for analysis. All additions were monitored gravimetrically to account for dilution. The diluted samples were analyzed on the ICP-MS using the standard ICP-MS protocol, except that $HNO_3$ was replaced with DDI water in order to improve detection of iodine. Sodium iodide standards were made for ICP-MS calibration in concentrations of: 1 ppb, 5 ppb, 10 ppb, 50 ppb, 100 ppb, 500 ppb, 1000 ppb, 5000 ppb, and 10,000 ppb (see calibration curve in appendix).

The equilibrated solid phase concentration of iodine was calculated using the following equation:

$$[I]_{sorbed,t} = \frac{\left([I]_{aq,0} - [I]_{aq,t}\right) * V_L * \frac{1\,L}{1000\,mL}}{m_{soil}} \quad [1]$$

Where: $[I]_{sorbed,t}$: Solid phase iodine concentration (µg/g) at time $t$

$[I]_{aq,0}$ : Initial aqueous iodine concentration (µg/L)

$[I]_{aq,t}$ : Aqueous iodine concentration (µg/L) at time $t$

$V_L$ : Sample liquid volume (mL)

$m_{soil}$ : Sample soil mass (g)

The solid-aqueous conditional distribution coefficient ($K_d$) was calculated using the following equation (Emerson *et al.,* 2014):

$$K_d = \frac{[I]_{sorbed}}{[I]_{aq}} \quad [2]$$

As seen in Emerson *et al.* (2014), $K_d$ changes with total iodine concentration. A true $K_d$ is measured at equilibrium and would be linear and independent of concentration. The conditional $K_d$ is measured before equilibrium is reached, and it will be termed as "$K_d$" throughout the study.

## 2.3 BATCH KINETIC SORPTION EXPERIMENTS

Kinetic batch sorption experiments were performed to gather information on the rates of iodine sorption and desorption in a wetland soil. Kinetic batch sorption experiments were completed in triplicate in 50 mL polypropylene centrifuge tubes containing 0.01 M NaCl background solution and 50 g/L of the SRS wetland soil and a total volume of 45 mL. Stable iodine ($^{127}I$) was spiked into samples as iodide or iodate at the following initial concentrations: 0 ppb, 50 ppb, 100 ppb, 500 ppb, and 1000 ppb (in units of ppb of iodide and ppb of iodate). These spiking concentrations are more typical of the concentrations of iodine contamination found in groundwater (Li *et al.,* 2013, Alvarez *et al.,* 2016); because these concentrations ICP-MS detection limit of iodine is higher than some of the initial iodine concentrations, samples were also spiked with a radioactive isotope of iodine ($^{125}I$). Iodine-125 was chosen for its relatively short half-life (59.407 days (chart of nuclides)), but the half-life is long enough to have measurable activity for the length of the experiment (unlike iodine-131 (8 day half-life)). Iodine-125

decays 100% via electron capture to tellurium-125, which is a stable isotope of tellurium (International Atomic Energy Agency, 2017). Each sample was spiked with 45,000 Bq $^{125}I$ in the same form of iodine as the starting species (i.e. iodide or iodate). The small amount of $^{125}I$ was assumed to be negligible in regards to the concentration of iodine in the sample, as it was merely used as a radioactive tracer. The $^{125}I$ concentration in each sample was 1,000 Bq/mL (1.55 ng/L).

Iodide-125 ($^{125}I^-$) spiking solution was prepared by diluting the stock carrier-free 125 iodide from Perkin Elmer to 4.53 mL and storing it in a 20 mL plastic bottle incased in lead shielding; the small initial volume of stock solution is unknown, and the total activity of the stock solution was $4.40 \times 10^7$ Bq. Next, a small portion of solution was removed and diluted with DDI water until it reached a suitable amount of radioactivity: 20 mL of 45,000 Bq/mL stock solution so that after spiking there would be 1,000 Bq/mL in each sample. One milliliter of iodide-125 solution was spiked into each sample.

Iodate-125 ($^{125}IO_3^-$) solution was prepared based on the concept of iodide oxidation to iodate in Fox *et al.,* (2008). Approximately 1.98 mL of the diluted $^{125}I^-$ solution was moved into a new glass bottle; the stock solution was diluted to 50 mL with DDI water to reach 45,000 Bq/mL of solution. An excess of potassium permanganate ($KMnO_4$) was added to the $^{125}I^-$ solution (0.0117 g $KMnO_4$) and allowed to react over a period of five days in the dark. Approximately 800 μg of 0.10 M manganese chloride ($MnCl_2$) was added to the solution. To enhance precipitation of manganese dioxide ($MnO_2$), the pH was adjusted from ~2 to a pH of ~5.5 using 110 μL of 1.0 M NaOH. The solution was still slightly purple, indicating that there was still $KMnO_4$ in solution, thus an additional

1300 μg of 0.10 M $MnCl_2$ was added to the solution until it began to clear up. Then the solution was poured into a 60 mL syringe and filtered to 0.45 microns into a clean glass bottle. A 0.5 mL sample of the solution was taken for analysis via liquid scintillation counter (LSC) by a Perkin Elmer Tricarb 4200 LSC; four milliliters of LSC cocktail was added to the sample before counting.

In order to check the speciation of the iodate solution, an excess of N-methyldi-n-octylamine (MDOA) resin (2.0 g) was added to the $^{125}IO_3^-$ solution; the solution was shaken vigorously by hand for five minutes and then set in a fume hood. The resin was added to remove un-oxidized iodide left in the $^{125}IO_3^-$ solution, leaving only $IO_3^-$ in the $^{125}IO_3^-$ solution. After allowing the resin to react for two hours, the solution was poured into a 60 mL syringe and filtered to 0.45 microns into a clean glass bottle. A 1.0 mL sample of the solution was taken and 4.0 mL of LSC cocktail was added for analysis on the LSC in order to compare the activity before and after the resin was added. There was a 33% decrease in activity after the resin was added, accounting for radioactive decay. Because of the excess resin that was added, it was assumed that the $^{125}IO_3^-$ solution was truly iodate and not iodide at this point. In order to replicate the same amount of activity as the $^{125}I^-$ kinetic batch sorption experiment, about 3.30 mL of $^{125}IO_3^-$ solution was spiked into each sample.

These kinetic experiments were sampled at one hour, three hours, eight hours, twenty-four hours, three days, seven days, two weeks, four weeks, eight weeks, and ten weeks in order to increase time resolution compared to previous batch experiments. The pH and oxidation-reduction potential of every sample were measured and recorded

during each sampling event. Samples were analyzed via LSC, and all measured activities were decay-corrected to the beginning of the sorption experiment.

Due to the possibility of iodine transforming to molecular iodine gas ($I_2$), these experiment were performed in a laboratory hood, and an air sampler was run during the entirety of the sampling events or any time the samples were open (i.e. when measuring pH and oxidation-reduction potential (Eh)). Once the manipulation of each sample was finished, the screw cap was placed on top and tightened to ensure a closed system. This was a conservative measure during the iodide kinetic batch sorption experiment, as the iodine in the system was spiked in the reduced form (as NaI) and was added to a reducing system. Therefore, there was a low probability that $I^-$ would oxidize and form $I_2$ (g). During the iodate experiment, there was a higher risk of $I_2$ (g) formation, as the iodine in the system was starting out in an oxidized form in a reducing system. Nevertheless, it was expected that little to no molecular iodine gas would form, and the activity is low enough that it would be unlikely to receive a significant radiological dose from inhalation of 125-iodine gas.

The fraction of aqueous $^{125}$I was calculated using the following equation:

$$[^{125}I]_{fraction,t} = \frac{(CR)_t / V_{s,t}}{(CR)_0 / V_{s,0}} \quad [3]$$

Where: $[^{125}I]_{fraction,t}$ : Fraction of aqueous $^{125}$I at time $t$

$(CR)_t$ : Count rate of $^{125}$I measured via LSC (counts per minute) at time $t$

$V_{s,t}$ : Volume of aqueous sample (mL) at time $t$

$(CR)_0$ : Initial count rate of $^{125}$I measured via LSC (counts per minute)

$V_{s,0}$ : Initial volume of aqueous sample (mL)

Stable iodine is expected to behave the same way as $^{125}$I, therefore it was assumed that the fraction of aqueous $^{127}$I was equal to the fraction of aqueous iodine-125. The concentration of aqueous $^{127}$I was then calculated using the following equation:

$$[^{127}I]_{aq,t} = [^{125}I]_{fraction,t} * [^{127}I]_{aq,0} \quad [4]$$

Where: $[^{127}I]_{aq,t}$: Aqueous concentration of $^{127}$I (µg/L) at time $t$

$[^{125}I]_{fraction,t}$ : Fraction of aqueous $^{125}$I (unitless) at time $t$

$[^{127}I]_{aq,0}$ : Initial aqueous concentration of $^{127}$I (µg/L)

A desorption step of the kinetic experiment was begun after ten weeks of sorption. Immediately following the last sorption sample, all batch samples were weighed and then centrifuged at 8000 rpm for 30 minutes. As much of the supernatant was removed as possible without disrupting centrifuged soil, leaving iodine-loaded soil and a small volume (~0.5 mL) of solution (Figure B1). The supernatant from the iodide experiment was discarded into radioactive waste, and the supernatant from the iodate experiment was kept in clean 50 mL polypropylene centrifuge tubes for iodine speciation analysis. The mass of soil and water in all batch samples was measured gravimetrically so that the remaining iodine in pore water could be accounted for. After the last sorption sampling event, approximately 30 mL of solution was left; for each sample, the amount of aqueous solution was determined individually and subsequently replaced with 0.01 M NaCl to maintain the same solids to liquid ratio for desorption. After adding the 0.01 M NaCl, samples were vigorously shaken by hand and vortexed until all soil compacted in the bottom of the tube had been resuspended. Initial aqueous iodine in the sample was

calculated based on the dilution of the small amount of solution leftover after removing supernatant. The kinetic desorption samples were taken following the same methods as the kinetic sorption samples at approximately the same time points.

In order to determine the concentration of organic matter in the aqueous phase during the kinetic batch sorption experiments, six samples were made to mimic the kinetic batch sorption experiment samples: 2.25 g of SRS wetland soil was weighed into 50 mL polypropylene centrifuge tubes and 45 mL of DDI water was added. All samples were put on a rotator. After twenty-four hours, three of the samples were removed, centrifuged, and the supernatant was transferred into 50 mL borosilicate glass bottle and stored in the refrigerator. The remaining three samples were left to equilibrate for ten weeks before centrifuging them and transferring the supernatant in the refrigerator. Total aqueous organic carbon content of all samples was determined via TOC analysis. Standards of hydrogen phthalate were prepared in concentrations of: 0.5 $mg_C$/L, 1 $mg_C$/L, 2 $mg_C$/L, 4 $mg_C$/L, 8 $mg_C$/L, 15 $mg_C$/L, 25 $mg_C$/L, and 50 mgC/L. Note that this is not a determination of organic matter content for the SRS wetland soil, but rather an estimation of the amount of dissolved organic matter in the kinetic batch sorption experiments.

## 2.4 IODINE SPECIATIES SEPARATION

### 2.4.1 Control Samples

In order to determine the species present in samples from the iodate kinetic batch experiments, iodine speciation was carried out based on methods adapted from Schwehr and Santschi (2003). The three main species of iodine being quantified in these samples

were iodide, iodate, and organoiodine. Separation of these three iodine species was possible using a resin consisting of MDOA (Grogan and DeVol, 2013).

Preliminary testing of the resin was performed on four separate control solutions in triplicate: iodide, iodate, 4-iodoaniline, and L-thyroxine. The two organoiodine standards - 4-iodoaniline and L-thyroxine - were chosen due to their high purity (>98%); 4-iodoaniline is also a representative refractory organic iodine species found in soil (Hu *et al.,* 2005). All control solutions were prepared in water such that the total iodine concentration should be the same for all solutions (approximately 1000 ppb total I). Each solution was sampled after preparation to confirm the initial concentration. Five milliliters of each sample was removed and filtered to 0.45 microns in order to determine if there was an effect filtration.

The MDOA resin has a sorption capacity of 7800 $\mu g_{iodine}/g_{resin}$, therefore an excess of MDOA resin was added to each control sample, (Grogan and DeVol, 2013). Most of the iodide is expected to sorb to the resin and be removed in this step. The solutions were vigorously shaken by hand for 5 minutes and put on a rotator to equilibrate for two hours. Upon taking the solutions off of the rotator, each solution was individually transferred into a 60 mL syringe and filtered to 0.45 microns into clean 50 mL centrifuge tubes. Approximately 5 mL of each sample was transferred into a clean 15 mL centrifuge tube for analysis by ICP-MS. The same ICP-MS protocol and sodium iodide standard concentrations were used for calibration as previously used for the batch sorption experiment.

Next, about 0.34 mL of 100 mM $NaHSO_3$ was added to reduce iodate to iodide. Each sample was shaken vigorously by hand for a few minutes and then approximately 0.23 mL of 500 mM HCl was added to each sample. The samples were left on a rotator to react overnight. Iodate was reduced to iodide by the following reaction (Grogan and DeVol, 2013, Kahn and Kleinberg, 1977):

$$IO_3{}^-{}_{(aq)} + 3HSO_3{}^-{}_{(aq)} \rightarrow 3SO_4{}^{2-}{}_{(aq)} + I^-{}_{(aq)} + 3H^+{}_{(aq)}$$

The next morning, about 0.010 g of MDOA resin was added to each sample, the solution were vigorously shaken by hand for 5 minutes and put on a rotator to equilibrate for two hours. Upon taking the solutions off of the rotator, each solution was individually transferred into a 60 mL syringe and filtered to 0.45 microns into clean 50 mL centrifuge tubes. Approximately 5 mL of each sample was transferred into a clean 15 mL centrifuge tube for analysis by ICP-MS. In this step, most of the iodate was expected to reduce to iodide and subsequently removed via sorption to the MDOA resin. All samples taken were analyzed by ICP-MS using the same ICPMS methods as the batch sorption experiments.

The same methods were used to separate the iodine species in the week ten samples from the iodate kinetic batch sorption experiment. Any iodine removed after adding the resin the first time was assumed to be iodide; concentration of iodide in the sample was calculated with the following equation:

$$[I^-] = [I]_{total} - [I]_{resin,1} \quad [5]$$

Where : $[I^-]$ : Concentration of iodide (µg/L)

$[I]_{total}$ : Concentration of total iodine in the sample (µg/L)

$[I]_{resin,1}$ : Concentration of total iodine after adding and removing the resin for the first time (μg/L)

Iodine removed after adding the reductant and then the MDOA resin was assumed to be iodate.

$$[IO_3^-] = [I]_{resin,1} - [I]_{resin,2} \quad [6]$$

Where : $[IO_3^-]$ is the concentration of iodate (μg/L)

$[I]_{resin,1}$ : Concentration of iodine after adding and removing the resin for the first time (μg/L)

$[I]_{resin,2}$ : Concentration of iodine after adding the reductant and then adding and removing the resin for the second time (μg/L)

The concentration of iodine remaining in the sample was assumed to equal the concentration of organoiodine ([I-OM]):

$$[I - OM] = [I]_{resin,2} \quad [7]$$

Due to the nature of the calculation, the mass balance is always equal to 100%.

There are several limitations of using these methods for iodine speciation analysis including detection limitations of the ICP-MS, approximating the required additions of $NaHSO_3$ and HCl, and indirect determination of iodine species. Due to the qualitative nature of the indirect methods used, the iodine species were operationally defined as the: iodide-rich fraction, iodate-rich fraction, and organoiodine-rich fraction. It was expected that most of the iodide would bind to the MDOA resin after the first addition, thus the iodide-rich fraction is the fraction bound to the MDOA resin. A majority of the iodate is expected to reduce after additions of $NaHSO_3$ and HCl. Therefore the reducible fraction

that binds to MDOA is operationally defined as the iodate-rich fraction. The remaining iodine in the sample after reduction is the non-reducible iodine, and it is operationally defined as the organoiodine-rich fraction.

### 2.4.2 Iodine Species Separation on Kinetic Batch Samples

In order to determine the species present after allowing iodate to equilibrate with the SRS wetland soil for ten weeks, the supernatant from the iodate kinetic batch sorption was kept for analysis on iodine speciation following the same protocol as that from the preliminary testing above. Iodine species separation was also analyzed on the triplicates with the two highest aqueous concentrations at the end of the iodide and iodate kinetic desorption experiments; only the two highest triplicates from each desorption experiment were chosen for speciation analysis because of the detection limitations on the ICP-MS.

The amounts of 5 mM $NaHSO_3$ and 20 mM HCl needed for reduction were based on the calculated aqueous iodine-127 concentration from the last sampling event. Excess $NaHSO_3$ and HCl were added to each sample; however, in order to prevent the $NaHSO_3$ from reducing additional organic matter, the excess amount of $NaHSO_3$ was limited to about 20% excess needed for reduction. If the organoiodine is reduced in this step, it could potentially bind to the MDOA resin and be removed, leading to a false increase in the amount of apparent iodate in the sample. Similarly, if too much additional HCl is added, it could lead to precipitation or coagulation of organic matter, leading to prematurely filtering out organoiodine when the resin is being filtered out. Due to the large range of iodine concentration between samples (0 ppb to 1000 ppb), the amount of

$NaHSO_3$ and HCl added were based on each triplicate of samples to minimize the risk of creating over-reducing conditions.

# 3. RESULTS AND DISCUSSION

## 3.1 SRS WETLAND SOIL CHARACTERIZATION

The average organic carbon content of the SRS wetland soil is 9.70% with a standard deviation of 0.06%; that is ten times the amount of organic matter in the SRS upland soil (Barber, 2017). In fact, after loss-on-ignition, the SRS wetland soil closely resembles the SRS wetland soil indicating that the base mineralogy is similar and the wetland soil has an accumulation of organic matter (Figure B1, Figure B2). One potential issue with the loss-on-ignition experiment is that only about 5 g of soil was used. Hoogesteen *et al.* (2015) suggests using at least 20 g of soil to account for variations in loss-on-ignition measurements. Organic carbon content estimations could possibly be improved by using a clay correction factor to account for structural water loss (Hoogsteen *et al.,* 2015).

The SRS wetland soil has an average native iodine concentration of 14.00 ppb with a standard deviation of 1.73 ppb. This amount of native iodine is potentially significant enough to require that it be accounted for in some experiments, especially the kinetic batch sorption experiments where added concentrations of iodide or iodate were low or there was no amendment of iodide or iodate. Furthermore, the speciation of native iodine remains unknown. Therefore, in analysis of the sorption data discussed below, the native iodine is assumed to be the same as that as the initially added species (iodide or iodate) and thus added into the total iodine in the system. There is a potential that the native iodine could be in the form of organoiodine. Bowley *et al.* (2016) found that native iodine in a wetland soil was a combination of iodide and organoiodine.

After allowing the SRS wetland soil to equilibrate in DDI water for one day, the average TOC concentration was 8.17 ± 0.67 parts per million ($mg_C/L$). After allowing the soil to equilibrate in water and in the dark for ten weeks, the average concentration of TOC was 16.69 $mg_C/L$ ± .25. Initially there is a large amount of organic matter that is released from the soil and then the rate of organic matter release slows drastically. Thus, in the conceptual model of iodine transformations discussed below, the potential for transformation of iodide/iodate to organoiodine is included

## 3.2 BATCH SORPTION EXPERIMENT

Iodide sorption increases with increasing amounts of wetland soil (Figure 2). This is expected due to the binding affinity for organic matter described in many other studies (Chang *et al.,* 2014, Schwehr *et al.,* 2009, Xu *et al.,* 2012). It is hypothesized that the driving factor in the difference in sorption between the SRS upland and SRS wetland soils is the amount of organic matter. The SRS wetland soil has approximately eight times the amount of organic matter compared to the SRS upland soil (Barber, 2017). The $K_d$ increases the most between day 3 and day 14, indicating that a majority of iodide sorption happens at or before these time points (Figure 2). At similar pH, Emerson *et al.* (2014) showed that at week 3 the $K_d$ for 1000 ppb spiked iodide was 22.47 mL/g, which is approximately twice as high as the $K_d$ measured on day 14 for 5000 ppb spiked iodine (Figure 2). Additionally, the $K_d$ measured on week 8 in Emerson *et al.* (2014) was sixteen times higher than the $K_d$ measured in this experiment (Figure 2). The "SRS wetland soil" used by Emerson *et al.* (2014) was a different soil and the spiked iodide concentration

was one-fifth of the concentration in this experiment, and that could account for some differences in sorption (Table 1).

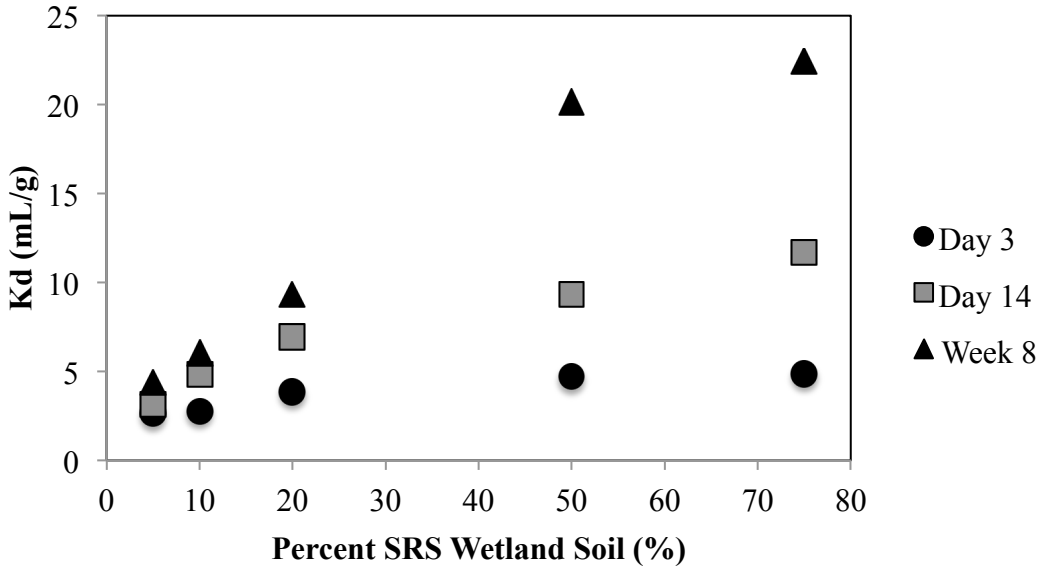


Figure 2. Percent SRS wetland soil versus $K_d$, three days, fourteen days, and eight weeks after spiking with stable iodide. The 100% SRS wetland soil data point has been deleted, as it is appears to be an outlier, most likely due to an error in accounting for the different soil moistures of the two different types of soil.

## 3.3 KINETIC BATCH EXPERIMENTS

### 3.3.1 SORPTION KINETICS

During the initial period of sorption, the fraction of iodide remaining in the aqueous phase demonstrates a large dependence on the total concentration of iodide in the system (Figure 3). However, at longer equilibration times, the variability in samples with different total iodide concentrations is minimized. The fraction sorbed is similar for all samples though a clear trend of decreasing sorption with increasing iodide concentration. A dependence of $K_d$ on total iodide concentration is a phenomenon that has been reported for iodide sorption in previous work (Emerson *et al.,* 2014, Zhang *et*

*al.,* 2011). Therefore, all $K_d$ values reported in this work should be considered as conditional values that are dependent on the equilibration time and concentration of iodine in the system. The data in Figure 3 also reveal that the sorption of initially iodide to this soil is not a first-order reaction. There are two apparent slopes for the four higher total iodide concentrations, which would indicate that this sorption process is at least a two-step reaction.

In comparison, iodate sorption exhibited relatively little dependence on the total concentration of iodate initially added to the system as shown in Figure 4. In the beginning of the experiment, iodate sorbs faster than iodide exhibiting greater sorption over the first 240 hours where aqueous iodate concentrations are lower than that of iodide for 100 ppb, 500 ppb, and 1000 ppb (Figures D12, D13). Samples with the lower concentrations of both iodide and iodate are comparable. At 240 hours, iodide concentrations are lower than that of iodide for the first time and continue until about 672 hours. For 1000 ppb initial concentration, the iodate data has a much larger standard deviation than the other two triplicates. The average pH for these three samples were 5.72, 5.37, and 5.31 with the highest value associated with the sample with the highest deviation. Therefore, some variation could be due to sample-to-sample variability. However, the data for this sample can be classified as an outlier using Grubb's test for outliers for some time points, but not others (Miller, 2015). Therefore it is included throughout the length of the experiment. Overall, the iodate data has a smoother curve than iodide. The iodide data has a linear decrease until 72 hours, then plateaus and slowly decreases from there (Figures D12, D13).

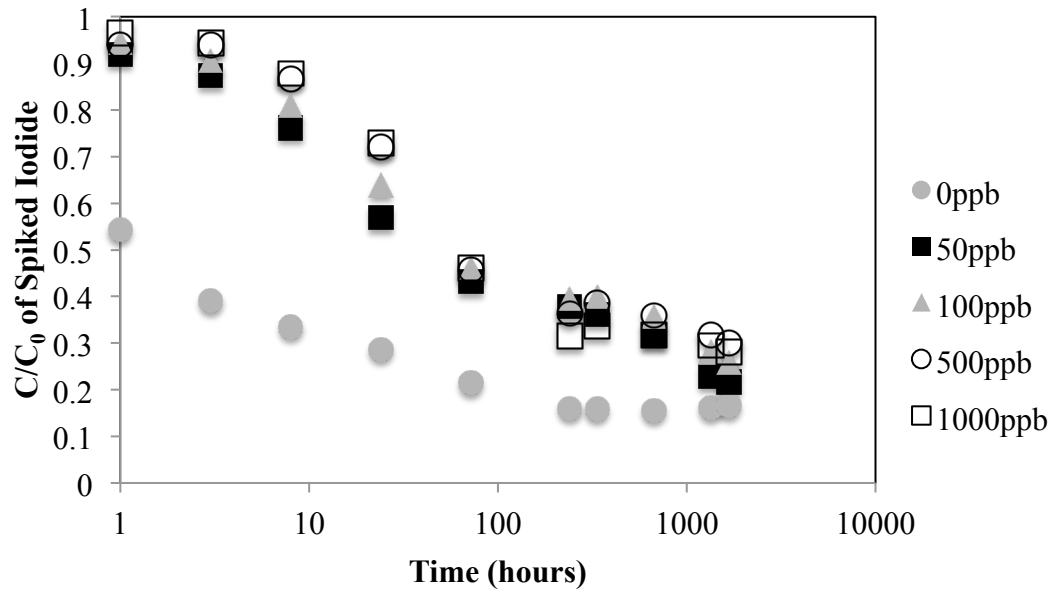


Figure 3. Normalized aqueous iodide concentration ($C/C_0$) over time during sorption of initially iodide to the SRS wetland soil. Note that the x-axis is on a log scale. Error bars are not shown for clarity. The average error for datapoints is 1.3%.

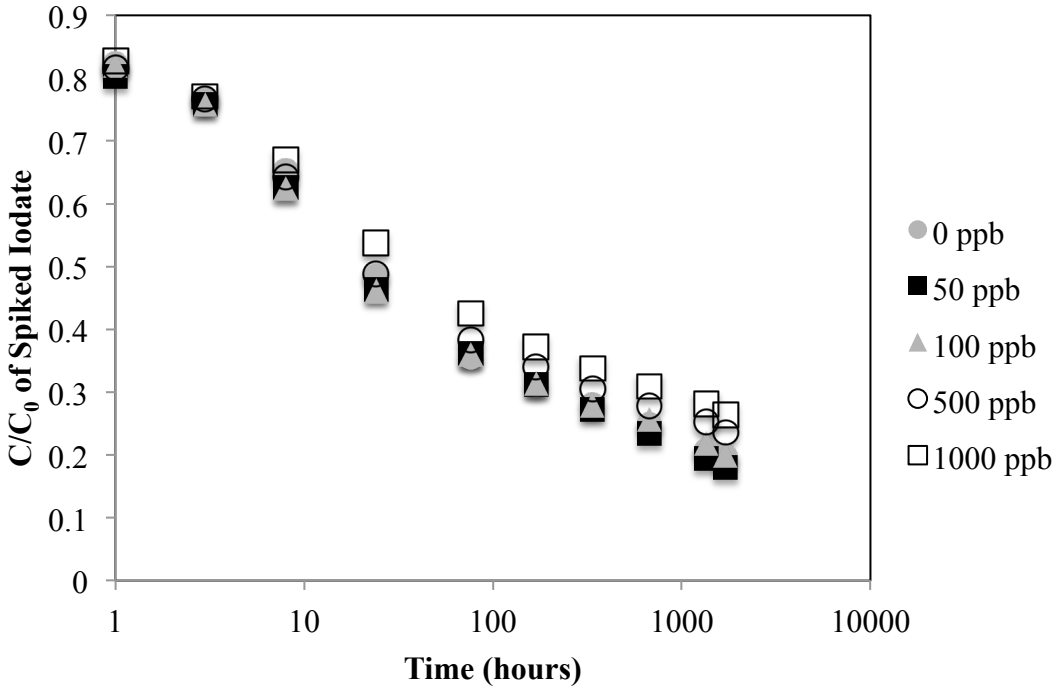


Figure 4. Normalized aqueous iodine concentration ($C/C_0$) over time during sorption of initially iodate to the SRS wetland soil. Note that the x-axis is on a log scale. Error bars are not shown for clarity. The average error for datapoints is 3.1%.

The most prominent observation about the normalized concentration plots is that the sorption is dependent on the concentration for both iodide and iodate (Figures 3, 4). Although the initially iodate data is more similar across concentrations at the same time point, the trend stays consistent throughout the experiment (Figure 4). The samples that had no iodide spiked into them (0 ppb) are different from the rest of the data. However, for initially iodate systems, the samples with no additional spiked iodate (0 ppb) data for iodate are about the same as the 50 ppb and 100 ppb data. The initially iodide data is a bit more irregular; the data across concentrations does not stay in the same order and the trend is disordered.

### 3.3.2 DESORPTION KINETICS

At the end of the sorption period, all samples (initially iodide and iodate) were centrifuged and the supernatant was replaced with iodine free 10 mM NaCl at pH 5.7 to initiate a desorption step. A remarkable finding from these experiments is the profoundly similar desorption behavior over a ten week period regardless of having iodide or iodate as the initial species at the start of the experiments (Figure 5). Due to the similar pattern of desorption, the iodine speciation is most likely converging to the same species of iodine regardless of the starting species. It is highly unlikely that the sorbed iodine would oxidize to iodate under the reducing conditions of the batch experiments based on the observed reduction potentials of these experiments and the stability fields of the iodide and iodate species (Pourbaix diagram and measured Eh-pH regions are shown in Appendix C figures C1 and C2). There are essentially no iodide-oxidizing bacteria in the

SRS F-area wetland sediments, and those few strains that do have the capability to oxidize iodide to iodate do so at a slow rate (Li *et al*., 2012). It is hypothesized that the iodate and iodide are converging to organoiodine on the surface of the soil, and therefore the sole desorbing species is organoiodine. Therefore, attempts were made to determine the speciation of the aqueous iodine following desorption.

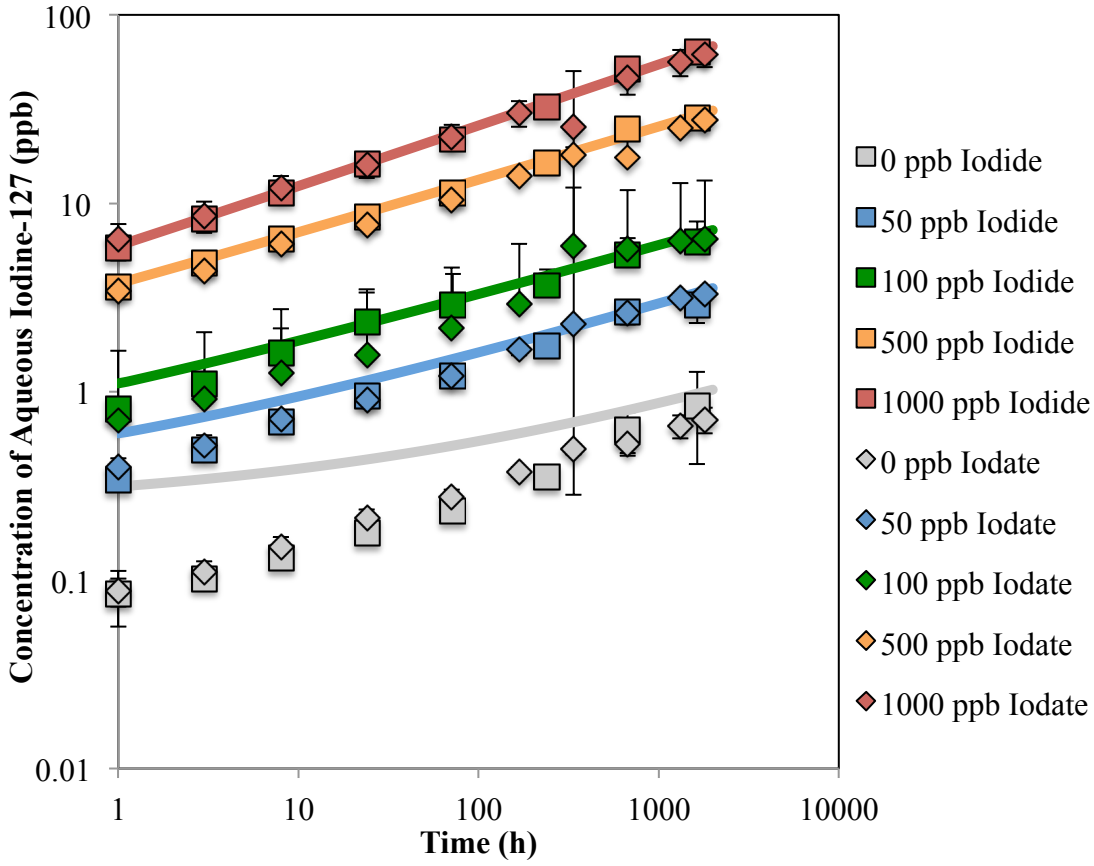


Figure 5. Concentration of aqueous stable iodine (ppb) over time during desorption from a soil that was equilibrated for ten weeks when iodide (squares) and iodate (diamonds) were initially added. The kinetic desorption numerical model for iodide is included (lines with no markers) in the figure and discussed in detail in section 4.2 below; the numerical model for iodate is similar to the model for iodide at the same concentration, so only one model was shown for simplicity. Note that both axes are on a logarithmic scale.

## 3.4 COMPARISON WITH EMERSON *ET AL*. (2014)

At artificially elevated iodine concentrations, Emerson *et al.* (2014) shows that $K_d$ varies with iodine concentration. Concentration-dependence of iodine sorption has been reported in other studies (Zhang *et al.*, 2011). Distribution coefficients are more consistent at ambient concentrations below 1000 ppb for iodide and iodate (Table 1, Table 2). Iodate exhibits a relatively smaller dependence on the total iodine concentration compared to iodide. The $K_d$s calculated in Emerson *et al.* (2014) are likely more of saturation effect rather than an effect of total iodine concentration on the amount of iodide and iodate sorption.

Table 1. Average $K_d$ at last sampling time point during kinetic batch sorption and desorption of initially iodide samples compared across all spiked concentrations and compared with Emerson *et al.* (2014). The average pH of the initially iodide kinetic batch sorption samples at ten weeks was 5.80.

| **Initial Iodide Concentration** | **Sorption $K_d$ (mL/g) at 10 Weeks** | **Desorption $K_d$ (mL/g) at 10 Weeks** |
|---|---|---|
| 0 ppb | 94.44 ± 24.03 | 1161.7 ± 297.64 |
| 50 ppb | 65.65 ± 3.89 | 2089.97 ± 469.82 |
| 100 ppb | 51.73 ± 3.62 | 1349.22 ± 501.29 |
| 500 ppb | 42.1 ± 0.85 | 971.46 ± 71.61 |
| 1000 ppb | 46.28 ± 1.11 | 1359.99 ± 319.8 |
| 1000 ppb* | 68.2 | N/A |

*Data from Emerson *et al.* (2014) at twelve weeks and pH 5.68

Table 2. Average $K_d$ at last sampling time point during kinetic batch sorption and desorption of initially iodate samples compared across all spiked concentrations and compared with Emerson *et al.* (2014). The average pH of the initially iodate kinetic batch sorption samples at ten weeks was 5.63.

| **Initial Iodate Concentration** | **Sorption $K_d$ (mL/g) at 10 Weeks** | **Desorption $K_d$ (mL/g) at 10 Weeks** |
|---|---|---|
| 0 ppb | 74.2 ± 15.21 | 1614.05 ± 234.94 |
| 50 ppb | 81.86 ± 7.71 | 1710.23 ± 489.61 |
| 100 ppb | 71.66 ± 4.2 | 1426.45 ± 223.59 |
| 500 ppb | 58.17 ± 5.1 | 1646.58 ± 175.86 |
| 1000 ppb | 53.55 ± 18.35 | 1842.37 ± 451.73 |
| 1000 ppb[a] | 145.28 | N/A |
| 10,000 ppb[b] | 9.15 | N/A |

[a] Data from Emerson *et al.* (2014) at twelve weeks and pH 5.81
[b] Data from Emerson *et al.* (2014) at twelve weeks and pH 5.74

## 3.5 IODINE SPECIATIES SEPARATION

### 3.5.1 IODINE SPECIATION OF CONTROL SAMPLES

Examining the apparent iodine speciation of >98% purity control samples was important in determining how well the iodine speciation separation method would work on samples. The L-thyroxine control sample showed that there is a potentially significant decrease in the iodine concentration after being filtered to 0.45 microns; none of the other controls seemed to be significantly affected by filtration. On average, 97% ± 0.3% of iodide was removed from the control containing 100% sodium iodide when the MDOA was added (Figure 6). About 19% ± 1.7% of the 100% iodate control sample appeared as iodide, 69% ± 0.5% appeared as iodate, and the remaining 11% of the sample appeared as organoiodine (Figure 6). In this closed system, it could be possible that a small portion of iodate could reduce to iodide. Although the results for iodate are not ideal, Grogan and

DeVol (2013) showed similar results for 100% iodate: 15% ±11% as apparent iodide and 79% ± 8% as iodate.

Initial total iodine concentrations of the organoiodine standards were lower than expected: 4-iodoaniline was half of the expected total iodine concentration, and L-thyroxine was only 48 ppb I out of the expected 1000 ppb I. This is most likely due to an error in making the control samples, but could also be related to the ability of the ICP-MS to ionize and detect these large molecular weight molecules. On average, 76% ± 2.1% of the 4-iodoaniline appeared as organoiodine. Only 44% ± 6.9% of the L-thyroxine was measured as organoiodine during the analysis. Both organoiodine standards contained an apparent 29% iodide. No iodate was detected in the 4-iodoaniline sample. However, the L-thyroxine standard had a measurement of 26% iodate (Figure 6). It is possible that the L-thyroxine was reduced to iodide and was removed during the addition of the MDOA resin after the reduction step, thus leading to an increase in the apparent iodate concentration. L-thyroxine's lowest pKa is 2.2 (Rumble, 2018) and the pH of the sample after adding the acid was 2.48. Therefore, it is possible that the negative charge on the L-thyroxine bonded to the MDOA resin and thus it was removed.

There is high uncertainty in the measurement of different iodine species using this indirect method of iodine speciation analysis. It is not possible to confidently quantify the distribution of iodine species in samples based on the abnormal results from the control samples. The apparent distribution of different iodine species in >98% pure control samples are most likely due to an error in the method used. However, it is possible to

compare the results of the iodine speciation analysis to the controls, and with the support of sorption and desorption data we can make predictions on speciation.

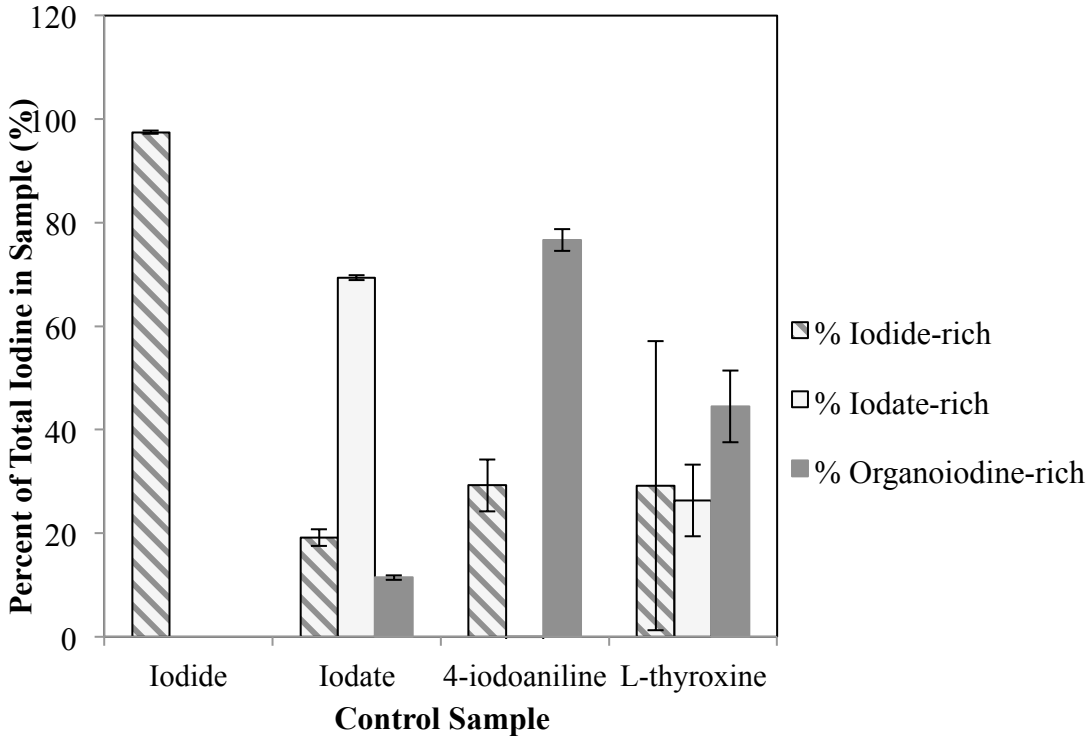


Figure 6. Iodine speciation of control samples in terms of percent of the initial total iodine concentration. Operational definitions of iodine species: iodide fraction (MDOA bound), iodate-rich fraction (reducible fraction that binds to MDOA), and organoiodine fraction (Total iodine – iodide rich – iodate rich).

### 3.5.2 IODATE WEEK 10 SORPTION SAMPLES

Iodine speciation separation was performed using the MDOA resin on the supernatant that was removed after ten weeks of sorption when iodate was initially spiked into solution. Iodate was expected to be present in these samples, as there was a measurable aqueous fraction of iodine in all samples at the time that the supernatant was removed (Figure 4). The percent of organoiodine formed decreases as the initial spiked

concentration increases, which is a trend that has been previously reported (Schwehr *et al.,* 2009). The high presence of organic matter in these samples indicates that iodate is sorbing to the soil, transforming to organoiodine and then the organoiodine is desorbing while iodate continues to sorb. The sample triplicate where no iodate was spiked shows that there is over 100% organoiodine, which is due to the error of the instrument (Figure 7). The soil used in Zhang *et al.* (2011) had a limited sorption capacity with iodide by

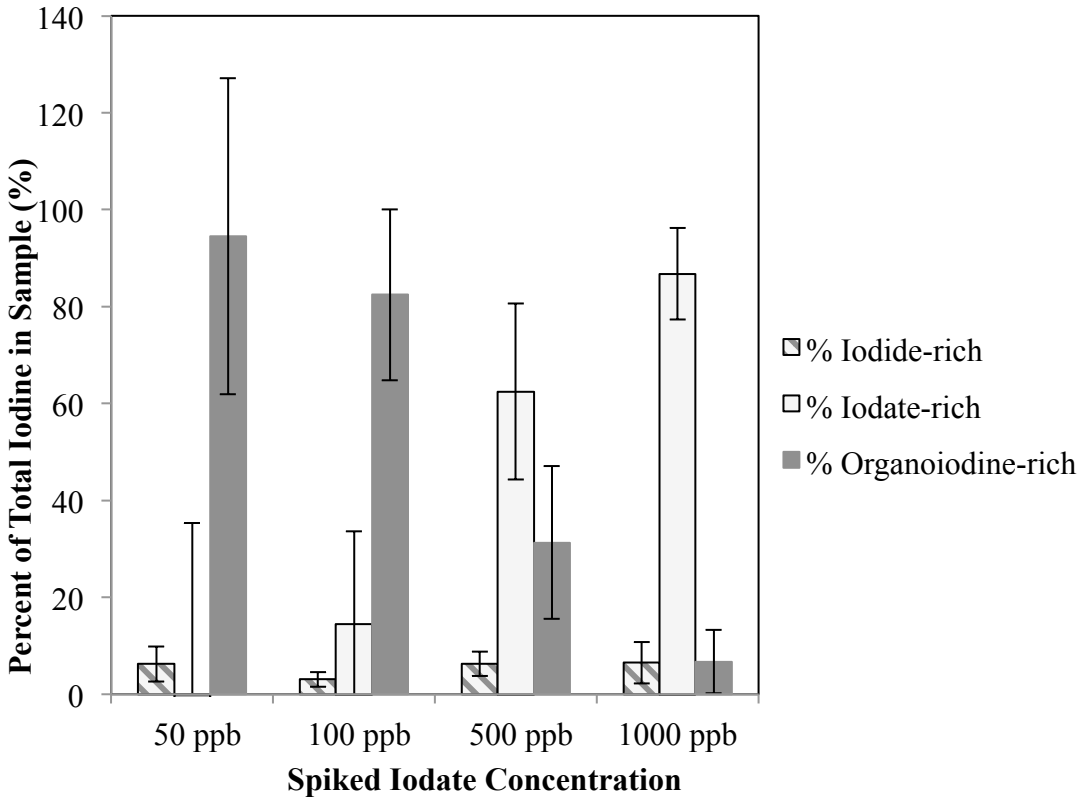


Figure 7. Percent of the initial total iodine concentration detected in each triplicate of samples from the supernatant removed at the end of the $^{125}IO_3^-$ kinetic sorption experiment (average of triplicate; error bars represent standard deviations). 0 ppb data is not included, because the concentrations were too close to the detection limits of the ICP-MS. Operational definitions of iodine species: iodide fraction (MDOA bound), iodate-rich fraction (reducible fraction that binds to MDOA), and organoiodine fraction (Total iodine – iodide rich – iodate rich).

irreversible covalent binding between 1 ppb and 10,000 ppb iodide; therefore it could be possible that the SRS wetland soil also has limited sorption capacity for iodine, which would also explain the decrease in percent organoiodine as the concentrations of spiked iodine increased. Figure 7 also serves as a reminder that the speciation of aqueous iodine is unknown throughout all batch experiments.

### 3.5.3 SPECIATION OF DESORPTION SAMPLES

After ten weeks of desorption, samples were centrifuged, filtered, and iodine speciation analysis was performed on the supernatant. At the end of kinetic desorption experiments in which iodide or iodate was initially spiked, there is a larger distribution of the different iodine species than expected (Figures 8, 9). The iodide kinetic desorption samples consist of mostly organoiodine (Figure 8). Organoiodine only accounts for 25% to 37% of the total iodine in the initially iodate samples (Figure 9). As discussed above, the speciation results cannot be considered to be a quantitative determination of the speciation due to potential overlap of the classification of iodine species from the indirect method utilized. However, qualitatively the results demonstrate that there are potentially iodide and iodate species present and that the desorbing iodine is not all present as organoiodine, which is the opposite of what was anticipated. The presence of iodide and iodate would only be possible if the organoiodine is reducing and/or oxidizing to iodide and/or iodate. These batch experiments are contained in closed centrifuge tubes, where oxygen is depleted quickly, and under these reducing conditions, it is highly unlikely that iodide and organoiodine are oxidizing to iodate (Figures C1, C2). Therefore, the

measurement of iodate is suspicious and potentially an experimental artifact. The apparent iodide in the desorption samples could potentially be accurate. However the iodine speciation separation on the organoiodine standards showed similar amounts of apparent iodide (Figure 6). Therefore it is possible that the iodide determined in these samples is due to removal of ionic forms of organoiodine as proposed for the L-thyroxine standard discussed above.

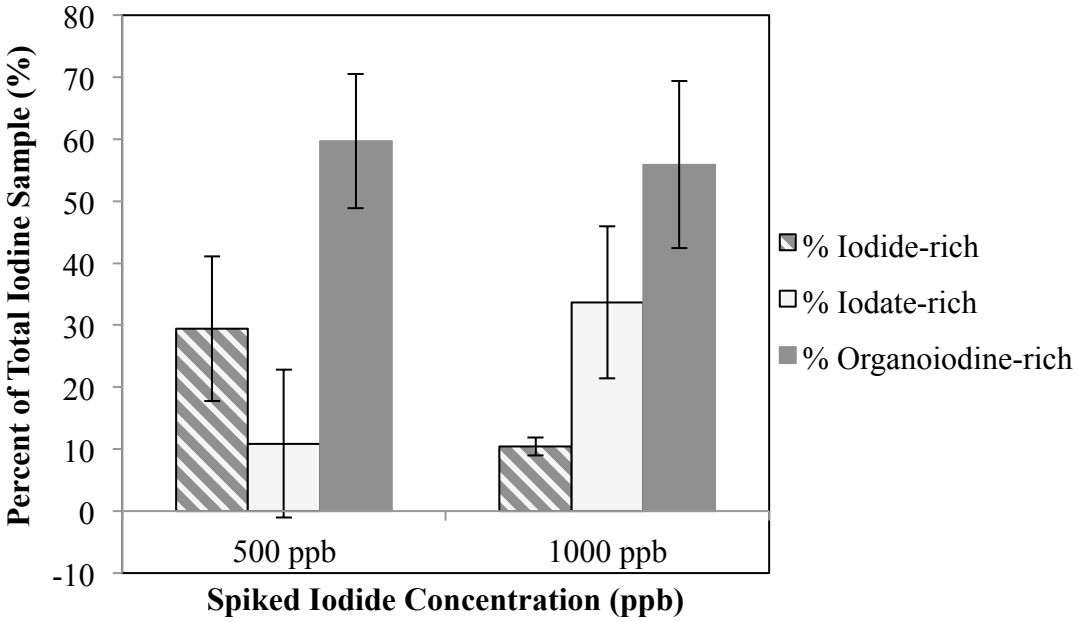


Figure 8. Percent of the initial total iodine concentration detected in samples at the end of the $^{125}I^-$ kinetic desorption experiment (average of triplicate samples; error bars represent standard deviations). Operational definitions of iodine species: iodide fraction (MDOA bound), iodate-rich fraction (reducible fraction that binds to MDOA), and organoiodine fraction (Total iodine – iodide rich – iodate rich).

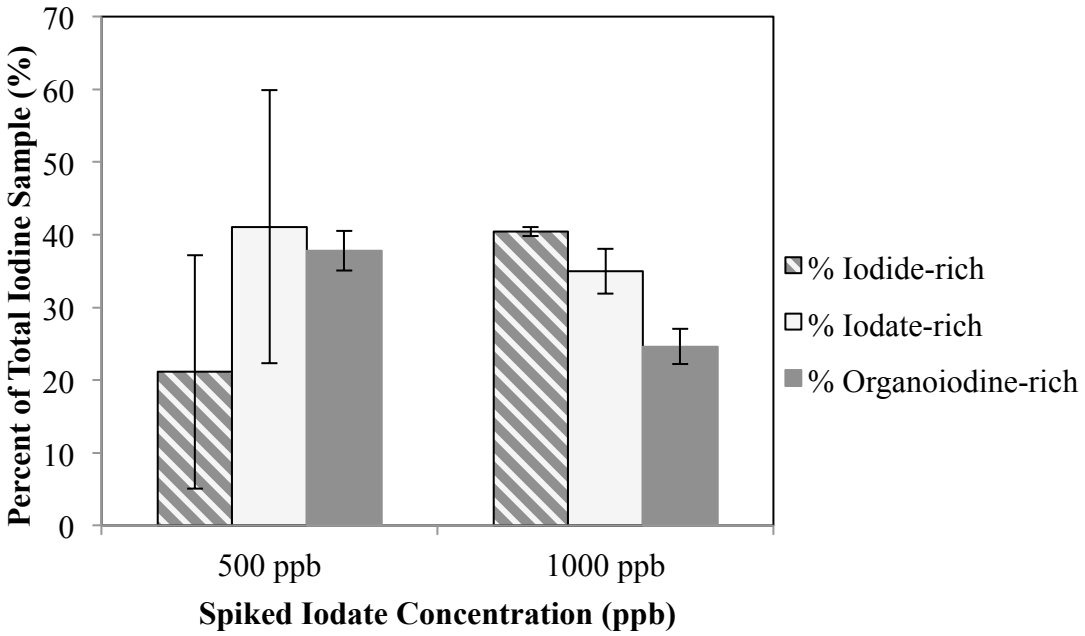


Figure 9. Percent of the initial total iodine concentration detected in samples at the end of the $^{125}IO3^-$ kinetic desorption experiment (average of triplicate samples; error bars represent standard deviations). Operational definitions of iodine species: iodide fraction (MDOA bound), iodate-rich fraction (reducible fraction that binds to MDOA), and organoiodine fraction (Total iodine – iodide rich – iodate rich).

The L-thyroxine standard had a similar distribution of iodine species, so it is possible that there was too much $NaHSO_3$ and HCl added for reduction (Figures 6, 8, 9). It is possible that the organoiodine is being reduced and subsequently removed via the MDOA resin after the reduction step Additionally, precipitation/aggregation of organic matter upon addition of the HCl could facilitate removal during solid-liquid separations of the resin or making iodine more difficult to detect on the ICP-MS. Due to the similar desorption behavior of the experiments where iodide and iodate were added, it must be true that these species are converging to the same species, and that species is highly likely to be organoiodine. A more direct means of determining iodine speciation in these

samples is required. However, development of such a technique is beyond the scope of this work.

### 3.5.4 IODATE SPIKED INTO TOC SAMPLES

The SRS wetland soil was allowed to equilibrate in water for one day and ten weeks in order to mimic the conditions during the kinetic batch sorption experiments, and those samples were analyzed to measure the amount of TOC in those samples (Table A1). Iodate was spiked into the remainder of the sample in order to determine if there was aqueous transformation of iodate to organoiodine. From Figure 8, Samples 1, 2, and 3 contained about 8.17 $mg_C/L$ of aqueous organic matter from the SRS wetland soil, and Sample 4 contained about 16.69 $mg_C/L$ of aqueous organic matter from the SRS wetland soil (Table A1, Figure A1). The oxidation-reduction potential measured during the iodate-125 kinetic batch sorption experiments (0.2286 V to 0.3095 V and pH of 5.05 to 5.68), indicate that aqueous iodate could reduce to aqueous iodide over the course of the experiment (Figures C1, C2). However, the control sample of iodate in water consisted of an apparent 19% iodide and 11% organoiodine, which indicate that the iodate spiked into the aqueous organic matter did not change speciation (Figure D1, Figure 10). The iodate spiked into the aqueous organic matter from the SRS wetland soil did not transform into organoiodine, indicating that the transformation between iodate and organoiodine does not occur in the aqueous phase. Therefore, in the conceptual model discussed below, it is assumed that formation of organoiodine occurs primarily on the soil surface.

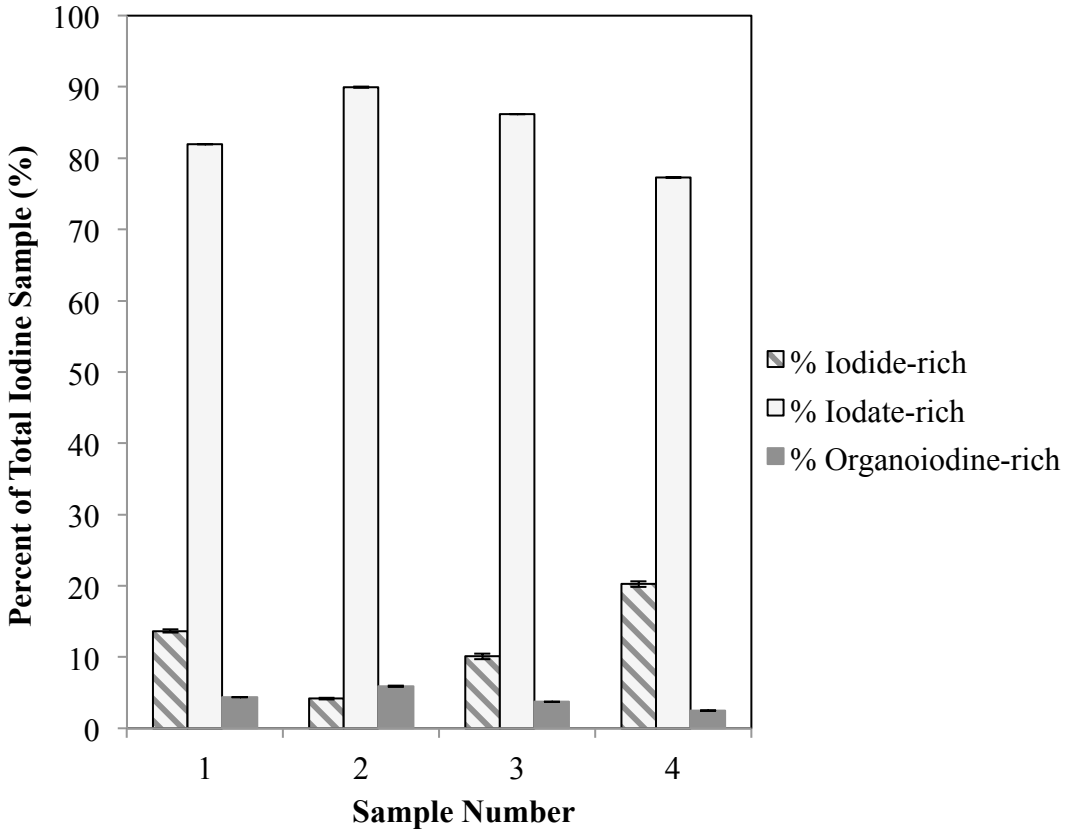


Figure 10. Percent of the initial total iodine concentration detected when 1000 ppb of stable iodate was spiked into aqueous organic matter from the SRS wetland soil, to mimic the conditions of the kinetic batch experiments (error bars represent standard deviations). Samples 1, 2, and 3 contained ~8.17 $mg_C/L$, and Sample 4 contained ~16.69 $mg_C/L$ of aqueous organic matter from the SRS wetland soil. Operational definitions of iodine species: iodide fraction (MDOA bound), iodate-rich fraction (reducible fraction that binds to MDOA), and organoiodine fraction (Total iodine – iodide rich – iodate rich).

# 4. KINETIC MODELING

## 4.1 CONCEPTUAL MODEL

A conceptual model was created in order to determine the possible transformations between aqueous iodine, organic matter, and soil and to determine which rate constants were controlling these transformations. This conceptual model serves as a foundation for defining a quantitative model. Simpler models were attempted to fit single-step zero, first, and second order reactions to the data (Appendix D). However, these single-step models did not fit the data well, and a more complex model was required for accurate representation of the data.

In the conceptual model, some terms were deemed to be unimportant in controlling the rates of transformation between aqueous and sorbed iodine. Significance was based on sorption data, desorption data, and iodine speciation of samples, which facilitated in narrowing down the reactions occurring in samples. Figure 11 depicts the prospective interactions between iodine (starting as iodide or iodate), organic matter, and soil. In this conceptual model, if there is a transformation between aqueous iodide and aqueous iodate, it is ignored; both of these species are treated as unspecified aqueous iodine and when sorbed, they are treated as unspecified sorbed iodine. The transformations between iodide and iodate are ignored because they are too complex to model and, based off of Figure 5, the initial aqueous iodine speciation does not matter in the rate of desorption. It is possible that iodate is reducing to aqueous iodide before sorption to the soil, and it is unlikely that iodide is oxidizing to iodate in the reducing environment of the kinetic batch experiments. The rate of desorption of iodine from the

soil into solution ($k_2$) is likely insignificant in comparison to 1) the rate of sorption of iodide or iodate from solution to the soil ($k_1$), 2) the rate of transformation of sorbed iodine to organoiodine ($k_3$), and 3) the reverse rate of that transformation reaction ($k_4$) (Figure 11). This assumption in based on the likelihood that formation of organoiodine complexes occurs irreversibly and that after formation of organoiodine occurs on the surface, desorption is controlled by the organoiodine species. It is noteworthy that this conceptual model has an inherent assumption of sorption hysteresis. If $k_2$ was significant, the one-step first-order reversible reaction model would have worked for the sorption data but as described in the fitting exercises of Appendix D, which was not the case. (Figures D1, D2, D3, D4, D5).

The reactions shown in figure 11 can be used to test various scenarios for development of a quantitative model using this conceptual framework. For example, the fact that the desorption behavior of initially iodide and iodate samples was similar indicates a similar speciation was achieved in both experiments. A corollary to this assumption is that the rate of surface-mediated transformation of sorbed iodine to organoiodine ($k_3$) is assumed to be fast relative to the desorption rate of organoiodine ($k_5$). If this was indeed the case, then the first-order reversible numerical model where $k_1$ is the forward reaction and the rate of desorption of the organoiodine complex ($k_5$) is the reverse would work in our data fitting routines. However, that was not the case as shown in figures D1, D2, D3, D4, and D5. It is likely that during the kinetic sorption batch experiment, the organoiodine is desorbing at the same time as iodide and iodate are sorbing as the system approaches equilibrium. In the last samples from the sorption

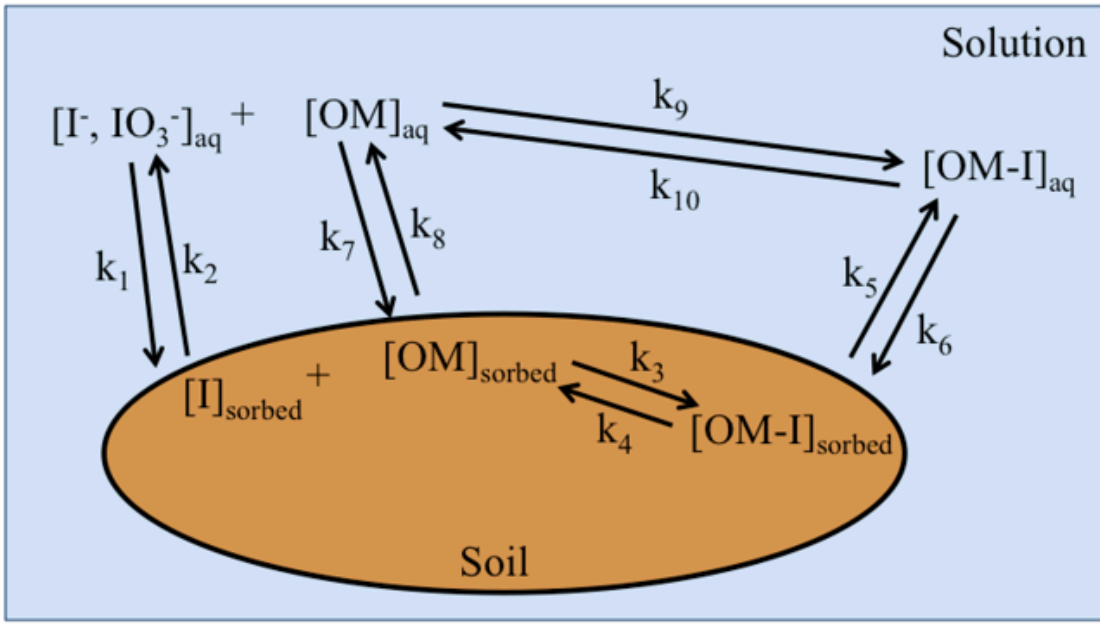


Figure 11. Conceptual model for iodine interactions with a high organic matter soil.

portion of the kinetic batch experiment, when the system was approaching equilibrium, it was found that a portion of the aqueous iodine was in the form of organoiodine; this phenomenon was more noticeable in the samples which had smaller amounts of iodate spiked into them (Figure 7). It has been reported that the covalent bond between iodine and soil organic matter is nearly irreversible (Kaplan *et al.,* 2014, Zhang *et al.,* 2011). Therefore, it is unlikely that the transformation of sorbed iodine and solid-phase organic matter to organoiodine ($k_3$) is a reversible reaction, thus $k_4$ is probably equal to zero. In the case that there is also iodide desorbing from the surface at the same time as organoiodine (possibly indicated by the presence of iodide in the iodine speciation results shown in Figures 8 and 9), $k_2$ would be important in the desorption step and $k_3$ would not be instantaneous. However, due to the similarities between the desorption of initially iodide and initially iodate kinetic batch experiments conducted months apart from each

other, it is more likely that the iodine is converging to one species – organoiodine - and that is the only iodine species desorbing from the surface of the soil (Figure 5). While this conceptual model is consistent with the data, it does not preclude the presence of a rate-limiting step ($k_3$) describing the formation of the surface bound organoiodine.

The iodate and aqueous organic matter speciation separation experiment showed that when iodate was spiked into the aqueous organic matter from the SRS wetland soil, the iodate did not transform into organoiodine after a period of three days. However, in one sample as much as 19% of the iodate seemingly reduced to iodide in that period of time (Figure 8). If the reaction between iodine and organic matter does not occur in the aqueous phase, $k_7$, $k_8$, $k_9$, and $k_{10}$ are not important and can be ignored (Figure 11).

Attempts were made to model the data using standard single step zero, first, and second order plots (Appendix D). The zero-order plots of the sorption data have two different slopes, which indicates the occurrence of two or more different sorption processes; the first several hours of sorption happens quickly and there is a second slower step after that (Figures D12, D13). This can happen for two reasons: 1) sustained aqueous concentrations are due to some reversibility, releasing some iodine (as iodide/iodate or, more likely, organoiodine) back into solution or 2) there is some concentration of reactive sites that is low and overcome at the point where the slopes change. The first reason is most likely true as evidenced by the fact that at the end of the kinetic batch sorption experiment with iodate, the two main species left in the samples were iodate (at higher spiked concentrations) and organoiodine (at lower spike iodate concentrations) (Figure 10). If the second reason were true, there would be a clear difference in sorption rates at

lower iodine concentrations; there would be a break where the reactive sites become saturated, which would happen more instantaneously at higher iodine concentrations. However, the normalized concentration plots are more similar across the different initial iodine concentrations (Figures 3, 4). Therefore, the driving rate constant for the net sequestration of iodine from the aqueous phase is the rate of sorption of iodine to soil ($k_1$) which is then essentially reversed by the desorption of sorbed organoiodine. The rate of desorption of iodine from a solid to solution is most likely driven by the rate desorption of the organoiodine species into the aqueous phase ($k_5$) until it reaches an equilibrium between the solid phase and aqueous phase ($k_5$, $k_6$) (Figure 11). Due to the uncertainty in the speciation analysis, the importance of $k_3$ and $k_4$ are unknown. Likely, they are important and the assumption of instantaneous formation of organoiodine is not correct. Therefore, a numerical model was developed to test this approximation and determine the reaction constants $k_5$ and $k_6$ from the desorption data. Given the uncertainty in the speciation of iodine on the solid phase, attempts to fit the forward sorption reactions ($k_1$, $k_2$) and solid phase transformations ($k_3$, $k_4$) were not performed.

## 4.2 NUMERICAL MODEL

As evidenced by the results of the iodine speciation analysis on the iodate kinetic sorption samples, organoiodine is desorbing during the sorption step (Figure 7). There is no speciation data during the kinetic sorption experiments to differentiate aqueous iodate from aqueous organoiodine that has desorbed from the surface of the soil. This makes

modeling sorption more complex to model. In order to determine sorption, desorption must be solved first, and the sorption model must be coupled with the desorption model.

MATLAB was utilized to create a numerical solution for desorption. Rates of iodine desorption are largely controlled by the rate of desorption of the sorbed organoiodine complex ($k_5$) and the rate of subsequent re-adsorption of aqueous organoiodine ($k_6$) (Figure 9). The change in concentration of aqueous organoiodine over time during desorption can be described by Equation 8:

$$\frac{\partial[I-OM]_{aq,t}}{\partial t} = -k_6 * [I-OM]_{aq,t}{}^{x} + k_5 * [I-OM]_{sorbed,t}{}^{y} \quad [8]$$

Where: $\partial[I-OM]_{aq,t}$ : change in concentration of aqueous organoiodine (ppb)

$\partial t$ : change in time (hr)

$[I-OM]_{aq,t}$ : aqueous organoiodine concentration (ppb)

$x$ : order of reaction for aqueous organoiodine (unitless)

$[I-OM]_{sorbed,t}$ : sorbed organoiodine concentration (ppb)

$y$ : order of reaction for solid-phase organoiodine (unitless)

All aqueous iodine measured during the desorption kinetic experiment is assumed to be in the form of organoiodine. Therefore, the concentration of aqueous organoiodine is equal to the concentration of aqueous iodine-127 (Figure 4, 9). The concentration of solid organoiodine was not directly measured; it was calculated by difference as shown in Equation 9:

$$[I-OM]_{sorbed,t} = [^{127}I]_{sorbed,0} - [I-OM]_{aq,t} \quad [9]$$

Where: $[^{127}I]_{sorbed,0}$ : concentration of $^{127}$I on the solid-phase at the beginning of the desorption kinetic batch experiment (ppb)

All terms in Equation 9 are in terms of aqueous concentration for modeling convenience, which is not entirely accurate. The real equation for the concentration of solid organoiodine is:

$$[I-OM]_{sorbed,t} = \frac{volume_{liquid}}{mass_{soil}} * ([^{127}I]_{sorbed,0} - [I-OM]_{aq,t}) \quad [10]$$

Similarly to the concentration of solid organoiodine (Equation 9) the solid concentration of iodine-127 was not directly measured; Equation 11 calculates sorbed $^{127}$I as:

$$[^{127}I]_{sorbed,0} = \left(1 - \frac{[^{127}I]_{aq,last}}{[^{127}I]_{aq,0}}\right) * [^{127}I]_{aq,0} \quad [11]$$

Where: $[^{127}\mathrm{I}]_{\mathrm{aq,last}}$ is the concentration of aqueous $^{127}$I for the last sampling event of the sorption kinetic batch experiment (ppb)

Utilizing MATLAB allowed for a numerical solution to Equation 8, solving for $k_5$, $k_6$, x, and y. The median data set (where 100 ppb was initially spiked into solution) for iodide desorption was chosen for optimizing the constants. For each data point, the model is calculated between the initial aqueous iodine concentration and the aqueous iodine concentration at time $t$, assuming that all data points in between do not exist. The constants x and y were manually fit using different combinations of 0, 1, and 2 until a good fit was found; x = 1 and y = 0 fit the trend of the experimental data the best. The resulting optimized rate constants were: $k_6 = -1$ ($h^{-1}$) and $k_5 = 0.2427$ ($[I\text{-}OM]_{aq}/h$). Plugging the optimized constants into Equation 8, yields Equation 12:

$$\frac{\partial[I-OM]_{aq,t}}{\partial t} = [I-OM]_{aq,t} + 0.2427 \quad [12]$$

Equation 12 was applied to the rest of the iodide desorption data and all of the iodate desorption data, and the resulting models seemed to predict the desorption trends for both iodine species at all concentrations. Some data points from the iodate kinetic desorption experiment (especially for the iodate 100 ppb, 500 ppb, and 1000 ppb) were far different from the general trend of desorption, and these points were excluded from the model calculation (Figure 4). Even when excluding these points from the model calculation, the model is within the standard deviations of these abnormal data points. The model appears to fit the iodate desorption data better than it fits the iodide data due to larger variances between triplicates (Figure 5). The model for iodide fits within the standards deviations for 100 ppb, 500 ppb, and 1000 ppb and at the lower concentrations, the model does not predict the data well for the first few time points. However, overall it is quite remarkable that a single set of rate constants give reasonable approximations to two separate datasets with five subsets of total iodine concentrations. The acceptable fit to this data supports the hypothesis that sorption of one species and desorption of a second are the rate limiting steps in the complex set of reactions under consideration. It could be that the specific species assumed to be present (i.e., aqueous iodide/iodate initially and aqueous organoiodine after sorption occurs) are inaccurate. Therefore, additional measurements are needed to verify this speciation. It is unclear at this point why sorption follows a first order approximation while desorption follows a zero order. Again, the detailed speciation analysis could provide some evidence of the implications of this fitting exercise.

Several attempts at kinetic modeling were made in order to estimate rate constants for sorption and desorption of iodine during the kinetic batch sorption experiments (Appendix D). Zero-order, first-order, and second-order plots of kinetic data were created in attempts to fit data (Figures in Appendix D). An analytical solution to the first-order reversible reaction was solved for both sorption and desorption (Equation 12, Davis *et al.,* 2018, Figures in Appendix D). From Davis *et al.* (2018), the analytical solution for a reversible first-order reaction is Equation 13:

$$\ln\left(\frac{[I]_t - [I]_{eq}}{[I]_0 - [I]_{eq}}\right) = -k * t \qquad [13]$$

Where: $[I]_t$ : concentration of aqueous iodine (ppb) at time $t$

$[I]_{eq}$ : concentration of aqueous iodine (ppb) at equilibrium

$[I]_0$ : initial concentration of aqueous iodine (ppb)

$k$ : combination of the forward and reverse reaction rate ($h^{-1}$)

$t$ : time (h)

It was determined that the sorption kinetics of the initially iodide and initially iodate were too different from each other, and they were too complex to model in the time allotted.

# 5. CONCLUSIONS

One of the most important findings is that the solid phase iodine species appears to be converging to the same species after a period of just ten weeks (Figure 5). Therefore, for performance assessment modeling, it may not matter which iodine species is initially present (i.e. iodide or iodate) as it will transform into the same species regardless of the initial speciation, i.e., it achieves a steady state with respect to iodine speciation. It is most likely that all of the iodine is becoming organoiodine via a surface-mediated process; however, this must be experimentally verified using a direct measurement tool. When iodate was spiked into the aqueous SRS wetland soil organic matter, the iodate was somewhat reduced to iodide, but there was essentially no organoiodine formation in the aqueous phase after three days. Based on this observation, a conceptual model was developed assuming that transformation of iodide or iodate to organoiodine occurs on the solid phase. Based on a conceptual model of the reactions proposed to be the rate-limiting steps, a quantitative model was developed which could describe the desorption data using the Equation 12:

$$\frac{\partial[I-OM]_{aq,t}}{\partial t} = [I-OM]_{aq,t} + 0.2427$$

This equation can be used to describe iodine release from iodine-loaded soil into groundwater at ambient conditions.

# 6. FUTURE WORK

In order to better understand iodine complexation with the SRS wetland soil, it is important to perform more detailed characterizations on the soil and organic matter. There are many associations between chemical composition of the subsurface soil and iodine sorption (Li *et al.,* 2013). Particle size analysis, cation-exchange capacity, anion exchange capacity, and specific surface area analysis could aid in understanding the sorption of iodine to the soil surface; ion exchange can be controlling factor in iodine sorption (Zhang *et al.,* 2011). Extractable iron and aluminum can influence iodide sorption, as well (Kaplan *et al.,* 2000, Hu *et al.,* 2005).

As for characterization of the organic matter, iodine is known to covalently bind to aromatic moieties in natural organic matter, therefore if we have an idea of the aromatic moieties in the soil organic matter, it could aid in understanding the formation of organoiodine. Fourier transform ion cyclotron resonance mass spectrometry of the organoiodine complexes formed in the SRS wetland soil would aid in understanding the transformations between iodine and organic matter (Xu *et al.,* 2013). The kinetic batch experiments did not investigate the effects of pH on iodine kinetics; pH is one of the controlling factors of iodine transport (Kaplan *et al.,* 2011, Emerson *et al.,* 2014). The combined effects of pH on iodine and organic matter would be interesting. All experiments performed were zero-dimensional in higher water-to-soil ratios than occur in the subsurface; it could be useful to perform transport experiments in soil columns of iodine. Now that we have an understanding of the basic kinetics of iodine sorption and desorption, transport experiments could be a way to test rate constants.

There was a high amount of error in the indirect iodine speciation analyses using the MDOA resin. More testing on control samples would be beneficial. Using the same indirect methods, iodine speciation evaluation could be improved by a correction factor such as the deconvolution algorithm in Grogan and DeVol (2013). A more quantitative iodine speciation analysis would be ideal for better understanding the chemical transformations occurring in the system, which would also give us more information for developing a better model.

# 7. APPENDICES

APPENDIX A: SPECIATION SEPARATION METHODOLOGY

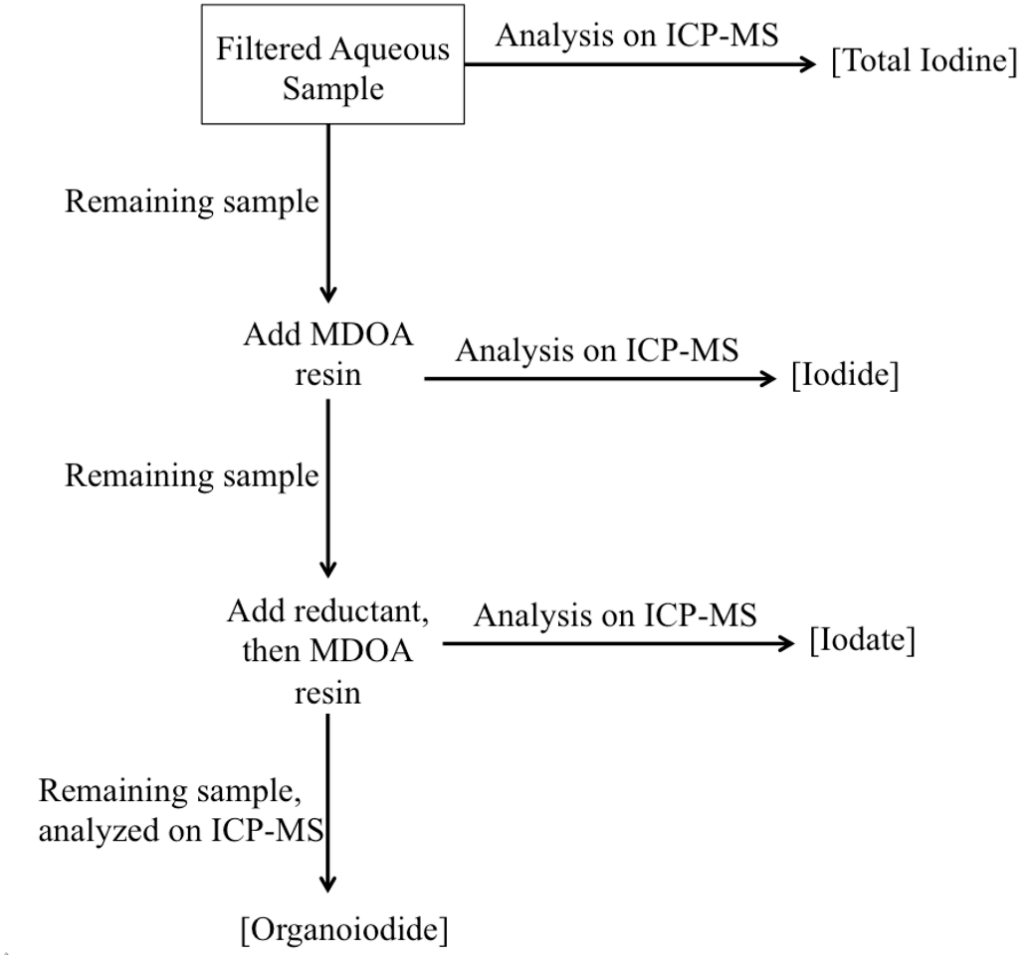


Figure A1. Methodical depiction for indirect determination of iodine species.

APPENDIX B: SRS WETLAND CHARACTERIZATION

Figure B1. SRS wetland soil (wet), before loss-on-ignition (left) and SRS wetland soil after loss-on-ignition (right).

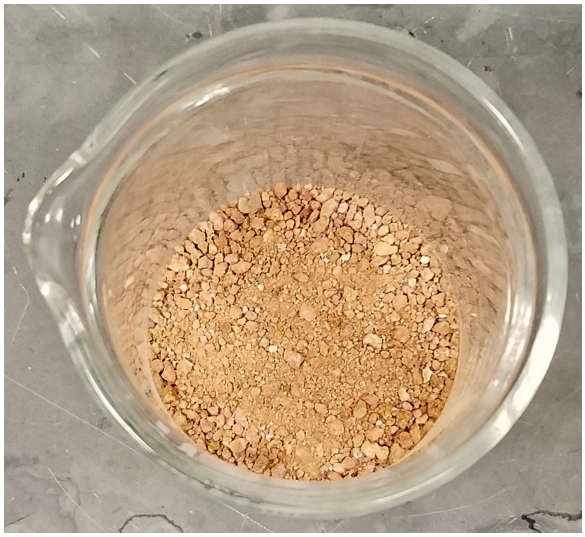

Figure B2. SRS upland soil.

Table B1. Total organic carbon calibration curve. Standards consisted of hydrogen phthalate.

| Standard | Total Organic Carbon Concentration ($mg_C/L$) | Peak Area |
|---|---|---|
| Standard 1 | 0.5 | 10.66 |
| Standard 2 | 1 | 14.57 |
| Standard 3 | 2 | 28.07 |
| Standard 4 | 4 | 54.11 |
| Standard 5 | 8 | 110.2 |
| Standard 6 | 15 | 208 |
| Standard 7 | 25 | 349.1 |
| Standard 8 | 50 | 703.6 |

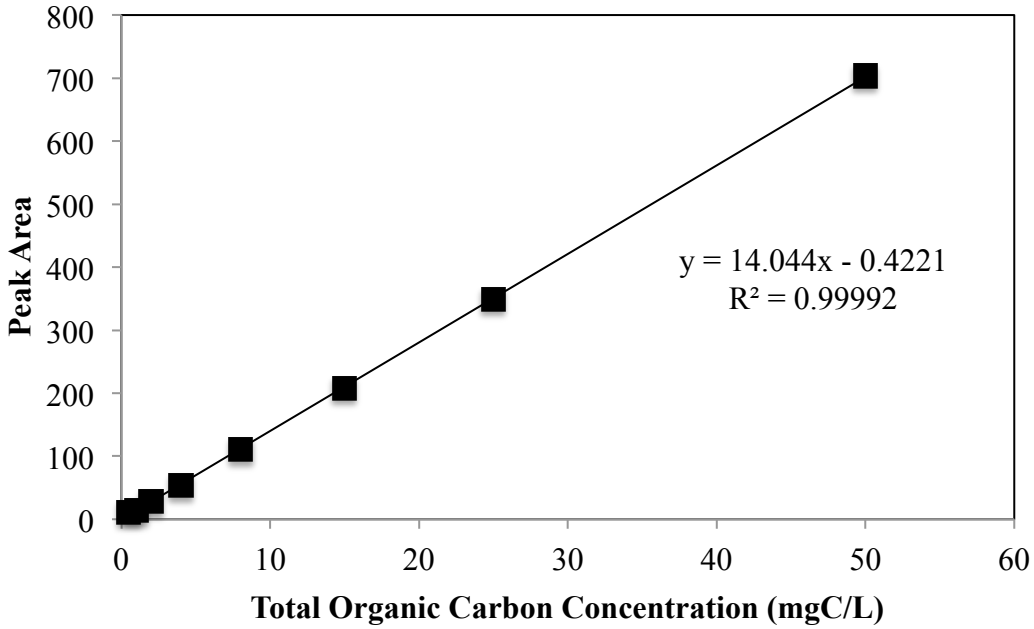


Figure B3. Calibration curve from total organic carbon analysis.

Table B2. Results of total organic carbon analysis on SRS wetland soil in water after equilibrating for one day and ten weeks; in order to protect the TOC instrument Week 10 samples were diluted in 1:1 ratio of sample to DDI water prior to analysis; thus the second column accounts for dilution.

| **Sample** | **Peak Area** | **Concentration of TOC in Sample Analyzed ($mg_C/L$)** | **Concentration of TOC in Original Sample ($mg_C/L$)** |
|---|---|---|---|
| Day 1_Sample 1 | 103.5 | 7.40 | 7.40 |
| Day 1_Sample 2 | 118.2 | 8.45 | 8.45 |
| Day 1_Sample 3 | 121.2 | 8.66 | 8.66 |
| Week 10_Sample 1 | 119 | 8.50 | 17.01 |
| Week 10_Sample 2 | 116.5 | 8.33 | 16.65 |
| Week 10_Sample 3 | 114.8 | 8.20 | 16.41 |

Table B3. Soil characteristics of SRS upland soil and SRS wetland soils used in Emerson *et al.* (2014) (Four Mile Branch wetland sediment) and this experiment (Tim's Branch wetland sediment).

| Parameter | Upland Subsurface Sediment (SRS Upland)* | Four Mile Branch Wetland Sediment (SRS Wetland in Emerson *et al.*, 2014)* | Tim's Branch Wetland Sediment (SRS Wetland) |
|---|---|---|---|
| Sand/Silt/Clay (% by weight) | 57.9/40.6/1.6 | 85.5/11.7/2.8 | - |
| Textural Classification | Sandy Loam | Loamy Sand | - |
| Equilibrium pH | 4.55 | 4.1 | 5.65 |
| Point of Zero Charge pH | 5.65 | 4.01 | - |
| Organic Carbon Content (% by weight) | 1.2 | 9.7 | 9.7 |
| Water Content (% by weight) | - | 43 | 21 |

*indicates data is from Emerson *et al.,* 2014

APPENDIX C: POURBAIX DIAGRAMS

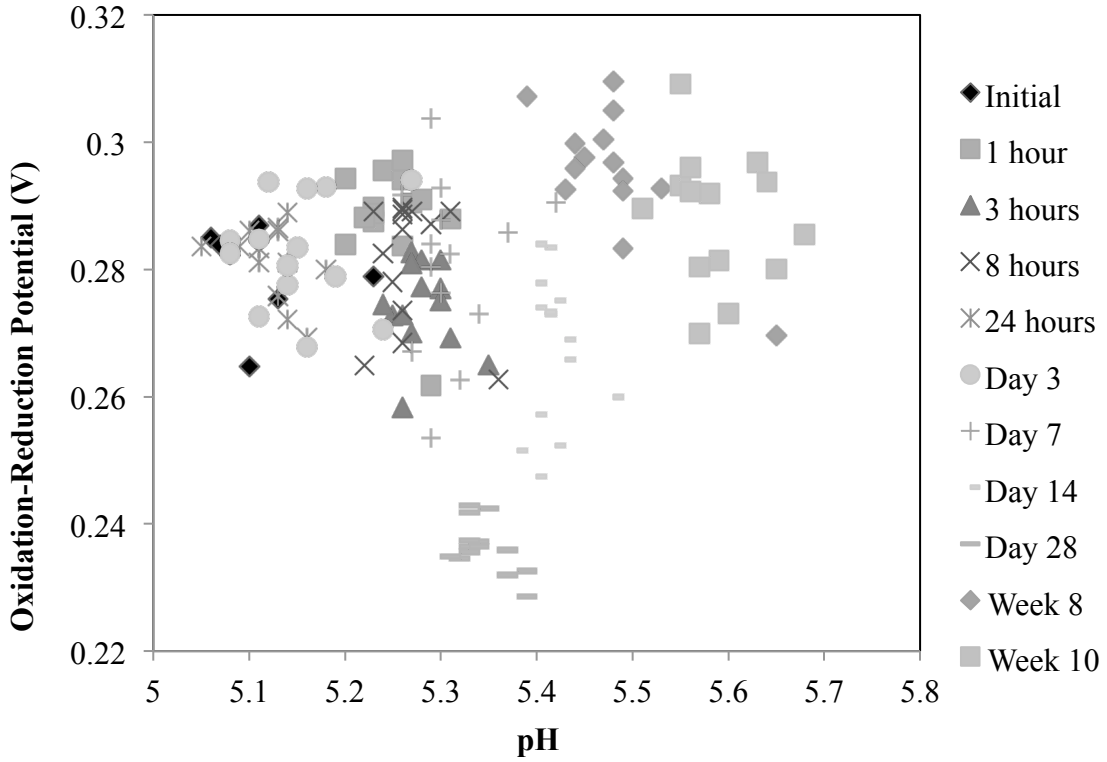


Figure C1. Eh and pH values measured during iodate-125 kinetic batch sorption experiments. Sample 10 (one of the triplicate samples in which 500 ppb of iodate spiked) has been omitted from this figure, because the measured pH and Eh are outliers from the rest of the data from each sampling event.

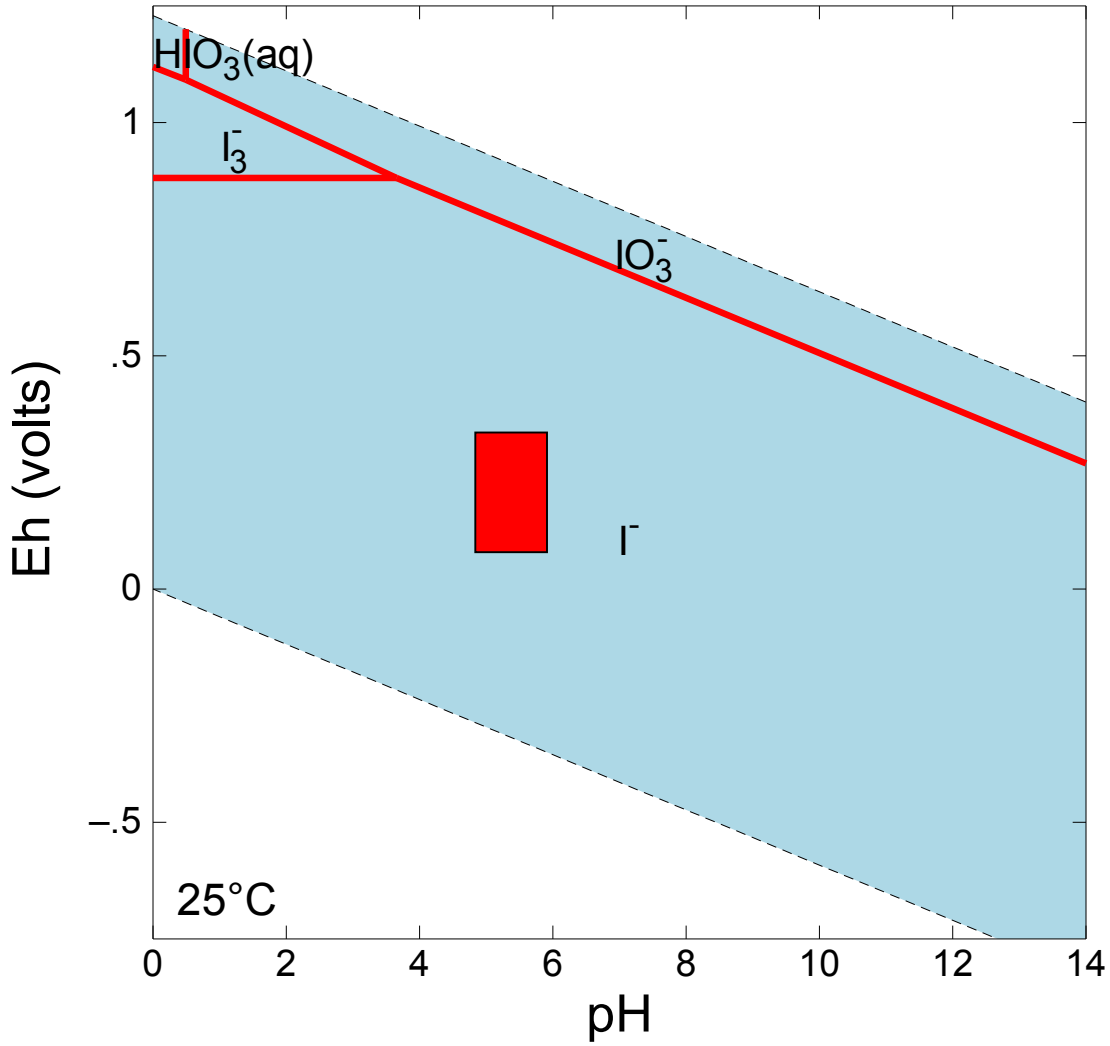


Figure C2. Pourbaix diagram for iodine species in water at 25°C. The red rectangle represents Eh-pH region of iodate sorption kinetic experiment (not exactly to scale).

## APPENDIX D: KINETIC MODELING ATTEMPTS

### REVERSIBLE FIRST-ORDER REACTION MODELING

The aqueous concentration of the last sampling point was assumed to be the equilibrium concentration. In order to determine first-order rate constants, the first-order data (aqueous concentration of $^{127}I$ for sorption and solid concentration of $^{127}I$ for desorption) was used to calculate the left-hand side (LHS) of Equation 12. The resulting data calculated from the LHS was plotted, and a linear trendline was fit to the data using Excel's built-in function. The slope of the line was assumed to be the rate constant (k), which is combination of the forward and reverse reaction. Then the right-hand side (RHS) of Equation 12 was calculated using the slope of the trendline (k) and the time (t). The RHS data (termed "model" in the figures below) was added to the plot of LHS data to see how well the model fit the data.

Sorption models did not fit well for iodide or iodate across all concentrations (Figures). The first-order sorption plots for iodide were comparable across 50 ppb, 100 ppb, and 500 ppb therefore only the 50 ppb plot is shown (Figure D2).

The rate constants for sorption of iodide were similar for the four highest concentrations of spiked iodide, resulting in an average rate of $2.58 \times 10^{-3} \pm 2.05 \times 10^{-4}$ $h^{-1}$ (Table); comparably, iodate sorption were similar across all concentrations, resulting in an average rate of $2.21 \times 10^{-3} \pm 1.19 \times 10^{-4}$ $h^{-1}$ (Table). There was no apparent relationship between concentration and first-order rate constant for sorption or desorption (Tables).

FIRST-ORDER SORPTION MODELS BASED ON EQUATION 12

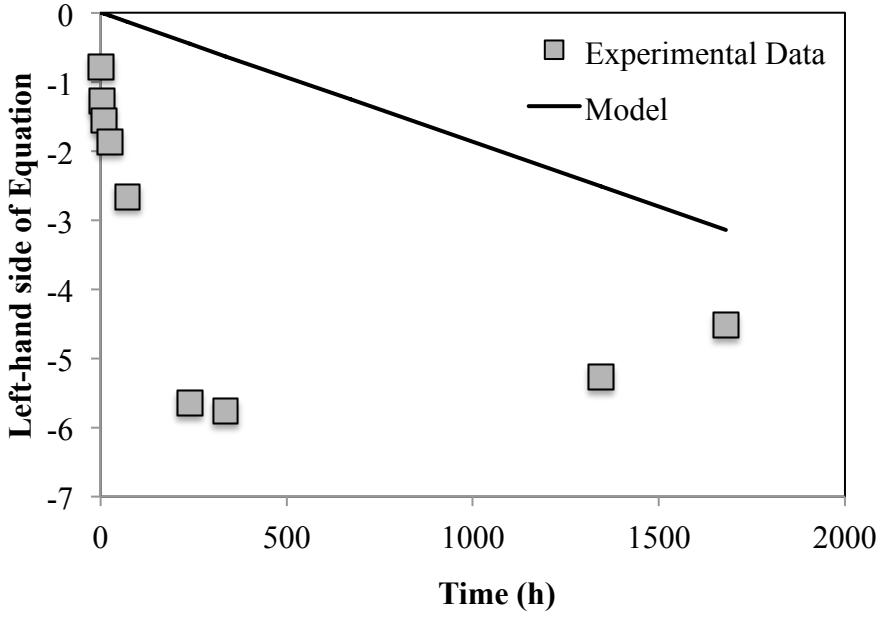


Figure D1. First-order model for sorption of aqueous iodide (aqueous) spiked with no additional iodide.

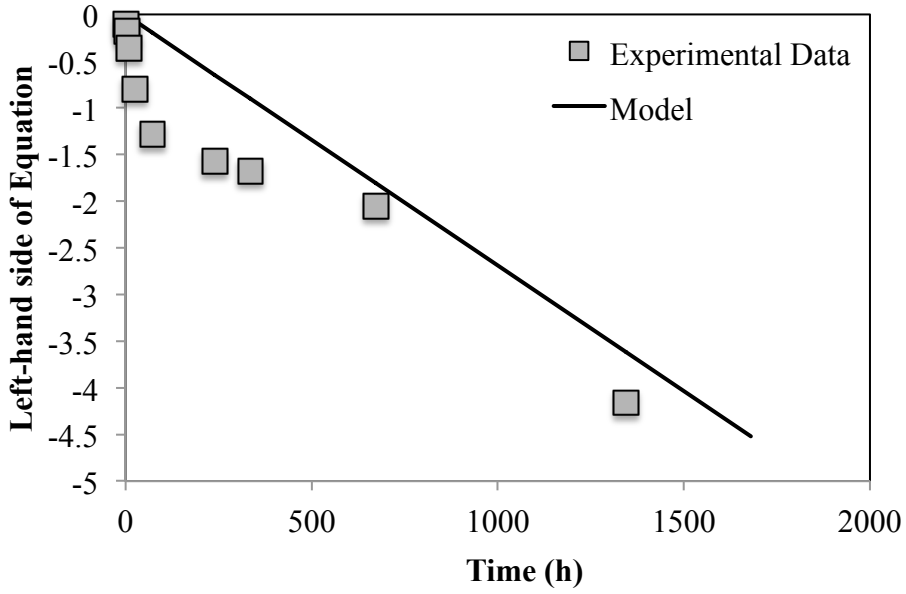


Figure D2. First-order model for sorption of aqueous iodide (aqueous) spiked with 50 ppb additional iodide.

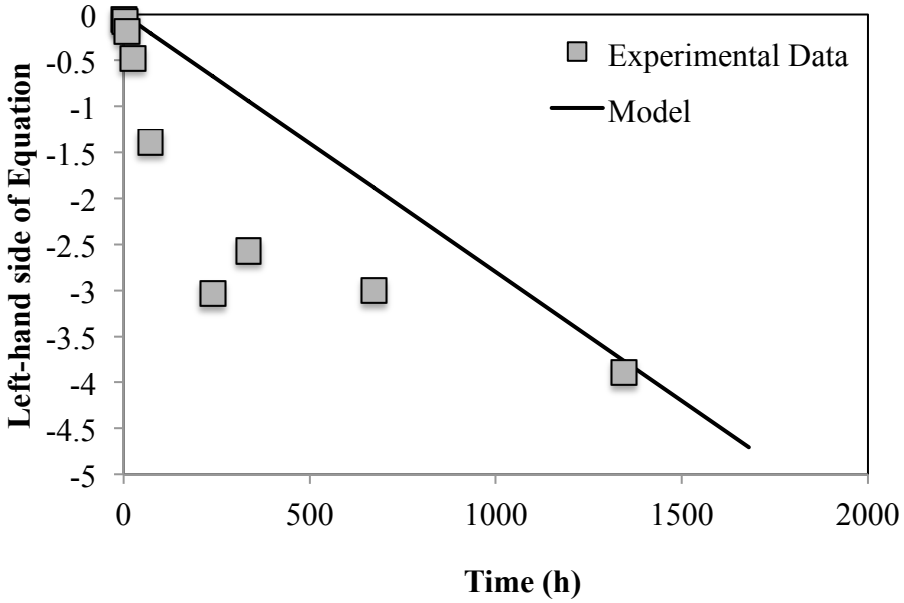


Figure D3. First-order model for sorption of aqueous iodide (aqueous) spiked with 1000 ppb additional iodide.

Table D1. First-order sorption rate constants for each initial concentration of spiked iodide.

| Initial Aqueous Iodine Concentration (ppb) | First-order Rate Constant (1/h) |
|---|---|
| 0 | 1.87E-03 |
| 50 | 2.69E-03 |
| 100 | 2.34E-03 |
| 500 | 2.50E-03 |
| 1000 | 2.80E-03 |

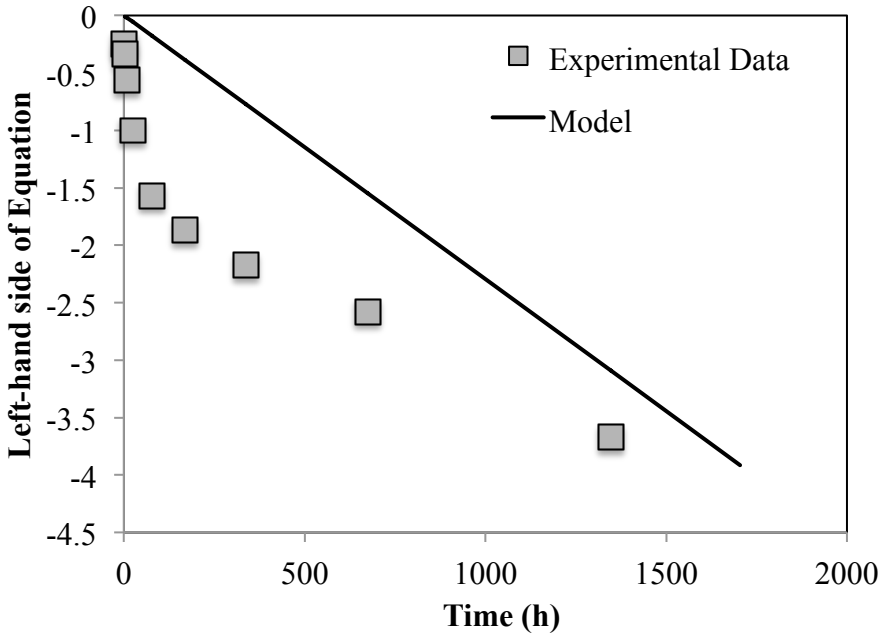


Figure D4. First-order model for sorption of aqueous iodide (aqueous) spiked with no additional iodate.

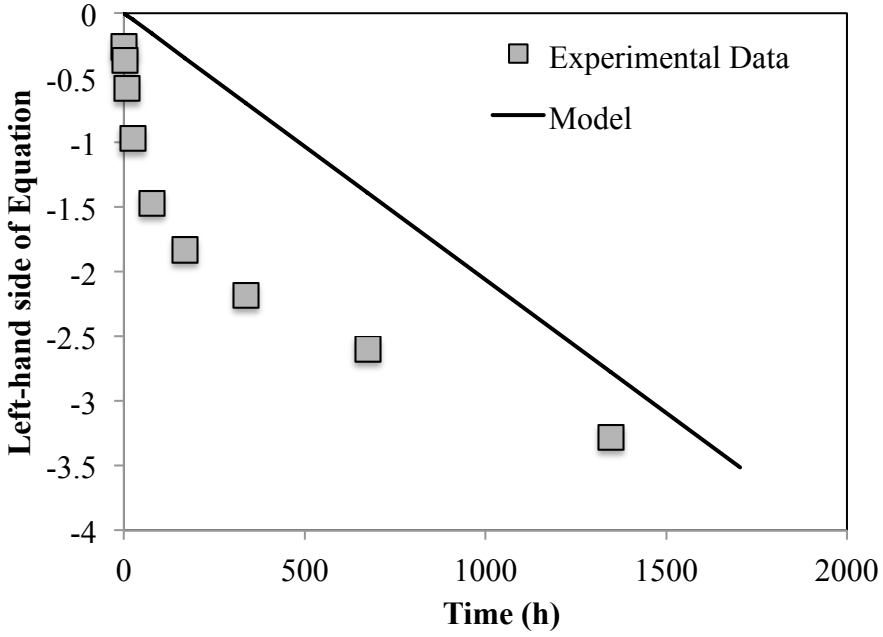


Figure D5. First-order model for sorption of aqueous iodide (aqueous) spiked with 1000 ppb additional iodate.

Table D2. First-order sorption rate constants for each initial concentration of spiked iodate.

| Initial Aqueous Iodine Concentration (ppb) | First-order Rate Constant (1/h) |
|---|---|
| 0 | 2.30E-03 |
| 50 | 2.36E-03 |
| 100 | 2.22E-03 |
| 500 | 2.13E-03 |
| 1000 | 2.06E-03 |

FIRST-ORDER DESORPTION MODELS BASED ON EQUATION 12

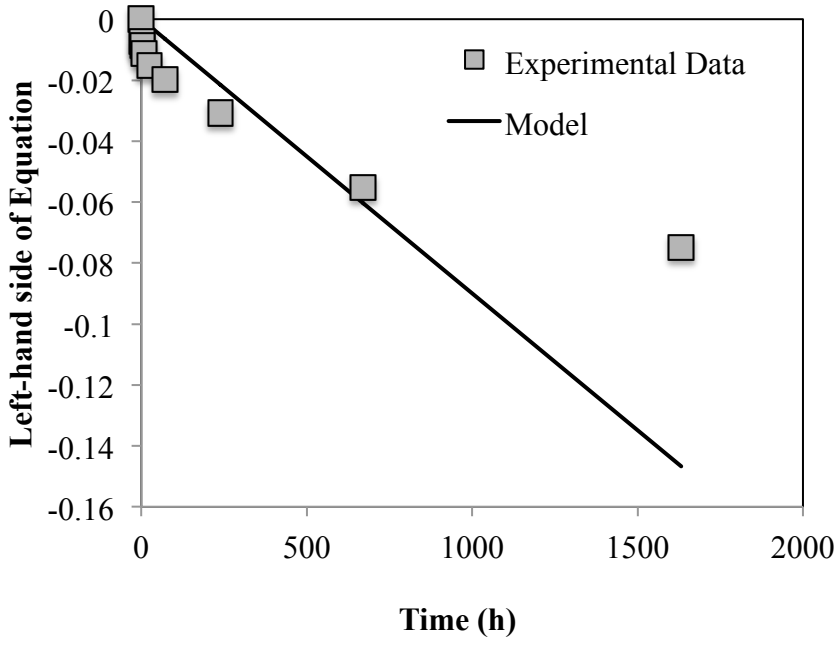


Figure D6. First-order model for desorption of iodine (sorbed) spiked with no additional iodide.

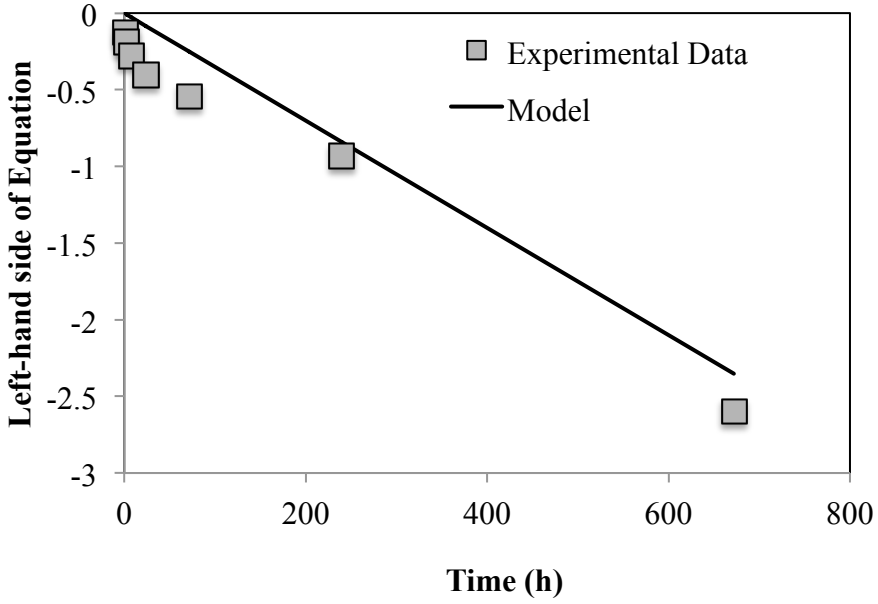


Figure D7. First-order model for desorption of iodine (sorbed) spiked with 50 ppb additional iodide.

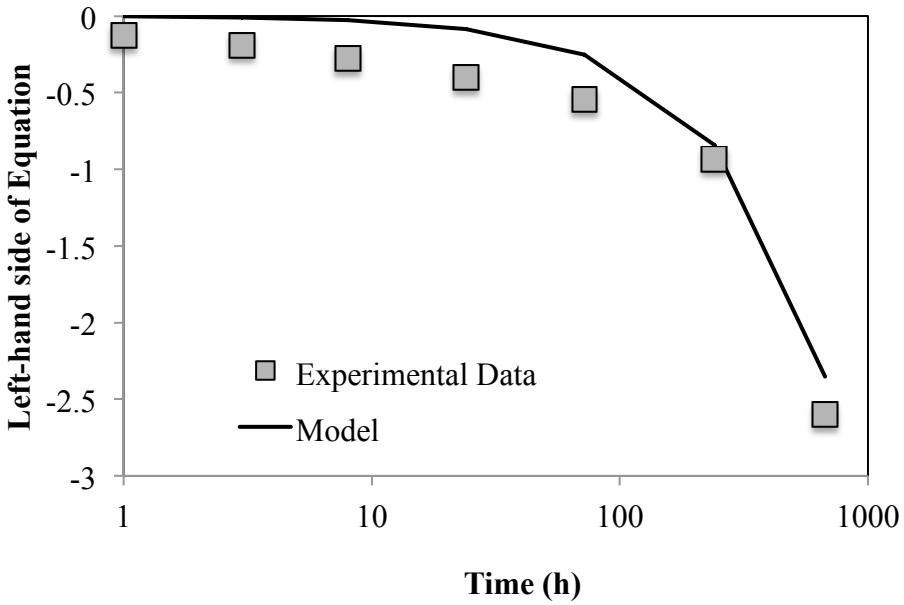


Figure D8. First-order model for desorption of iodine (sorbed) spiked with 50 ppb additional iodide with the x-axis on a logarithmic scale in order to better visualize the fit of the model.

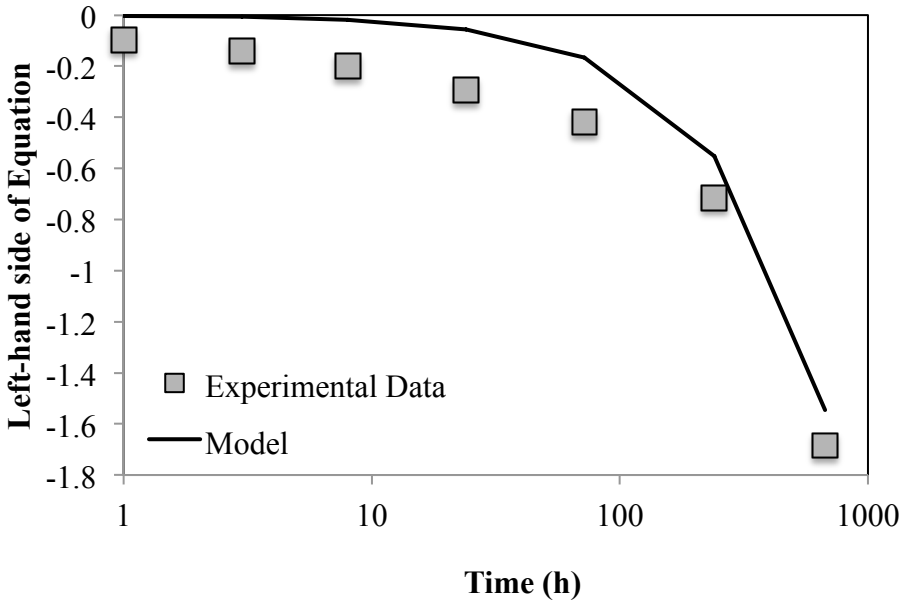


Figure D9. First-order model for desorption of iodine (sorbed) spiked with 1000 ppb additional iodide with the x-axis on a logarithmic scale.

Table D3. First-order desorption rate constants for each initial sorbed concentration of iodide.

| Initial Solid Iodine Concentration (ppb) | First-order Rate Constant (1/h) |
|---|---|
| 11.68 | 8.99E-05 |
| 50.21 | 3.50E-03 |
| 84.46 | 2.40E-03 |
| 358.79 | 2.90E-03 |
| 722.33 | 2.30E-03 |

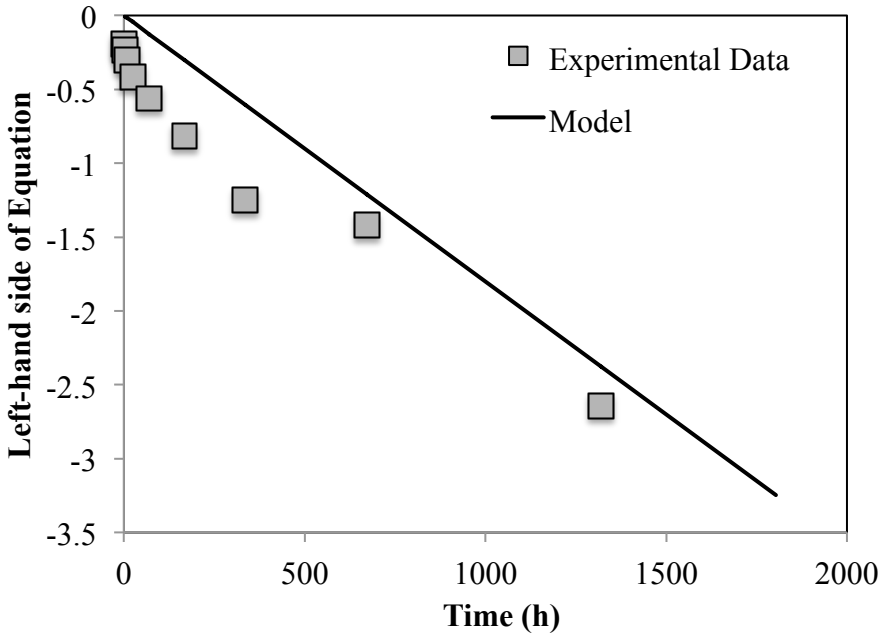


Figure D10. First-order model for desorption of iodine (sorbed) spiked with no additional iodate (0 ppb).

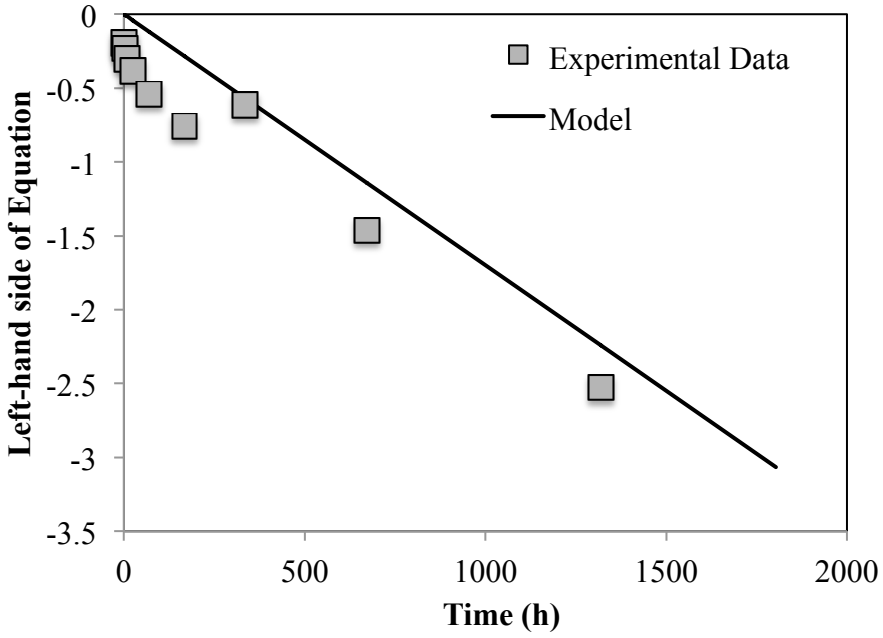


Figure D11. First-order model for desorption of iodine (sorbed) spiked with 1000 ppb additional iodate.

Table D4. First-order desorption rate constants for each initial sorbed concentration of iodate.

| Initial Solid Iodine Concentration (ppb) | First-order Rate Constant (1/h) |
|---|---|
| 11.23 | 1.80E-03 |
| 54.32 | 2.30E-03 |
| 92.60 | 2.50E-03 |
| 400.40 | 1.60E-03 |
| 761.14 | 1.70E-03 |

ZERO-ORDER SORPTION:

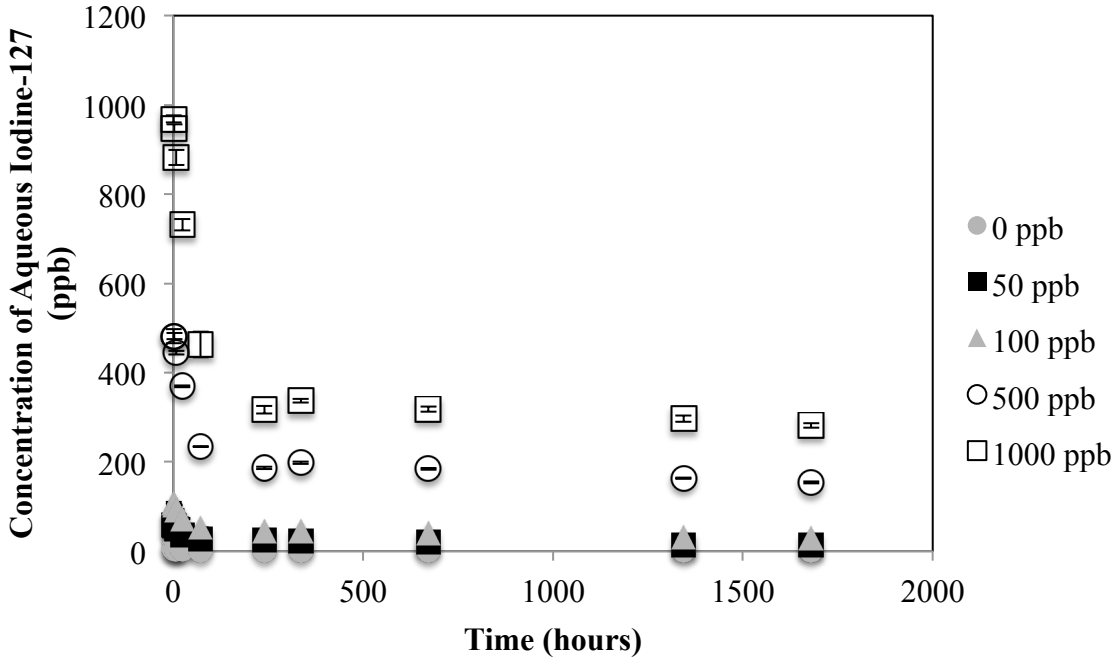


Figure D12. Zero-order model for sorption of iodide (aqueous).

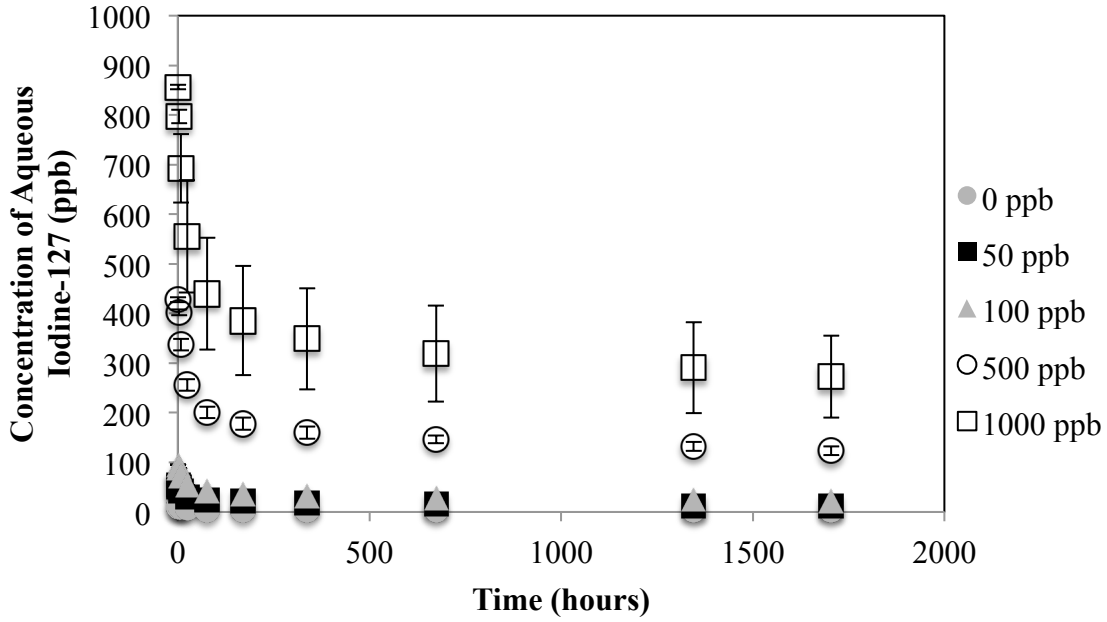


Figure D13. Zero-order model for sorption of iodate (aqueous).

SECOND-ORDER SORPTION:

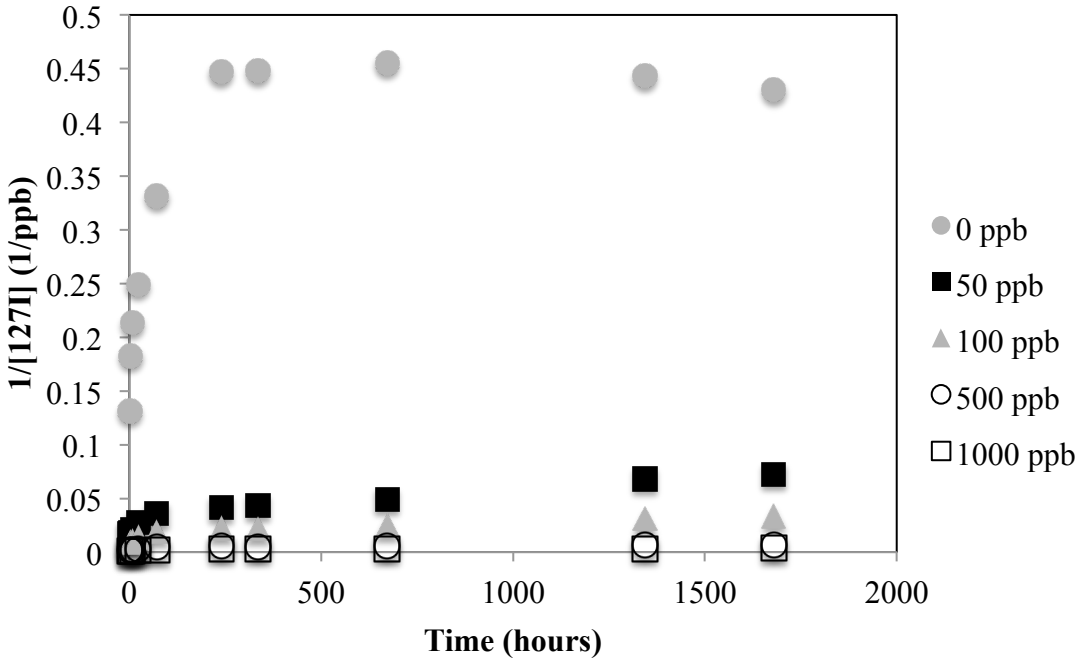


Figure D14. Second-order model for sorption of iodide (aqueous).

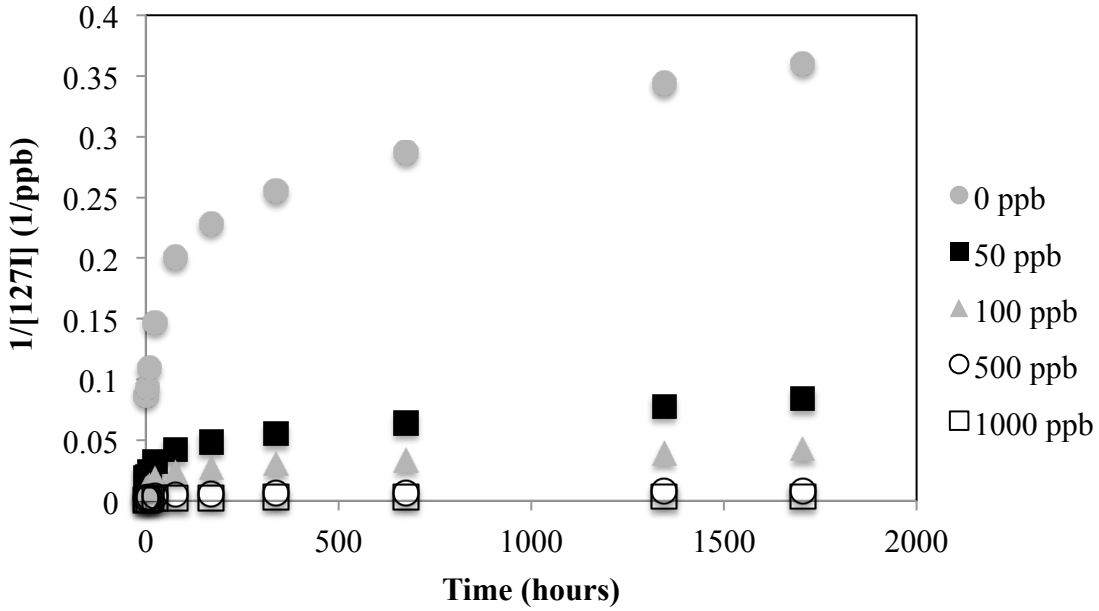


Figure D15. Second-order model for sorption of iodate (aqueous).

ZERO-ORDER DESORPTION:

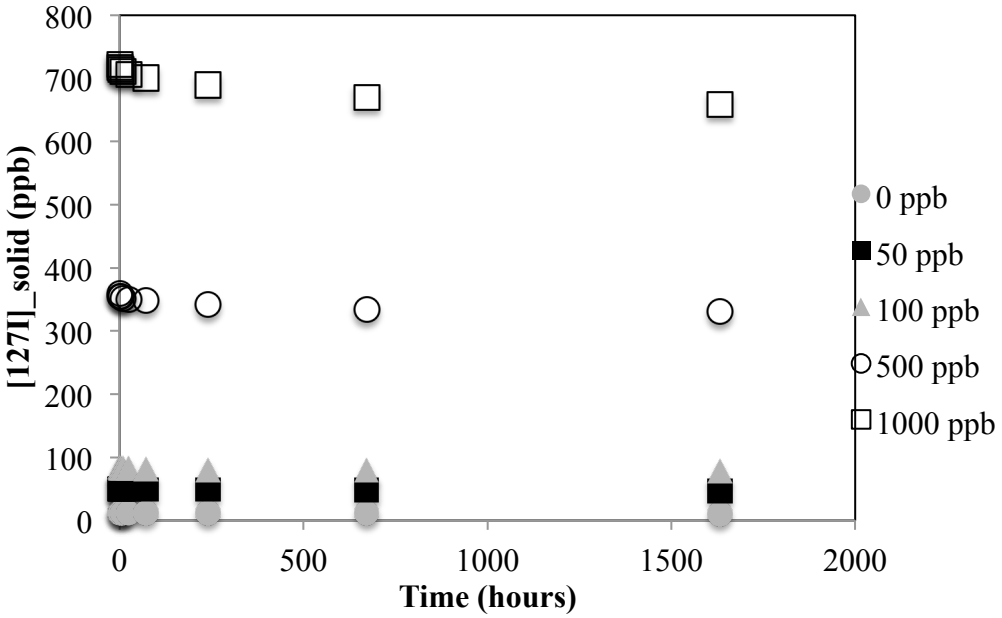


Figure D16. Zero-order model for desorption of iodide (sorbed).

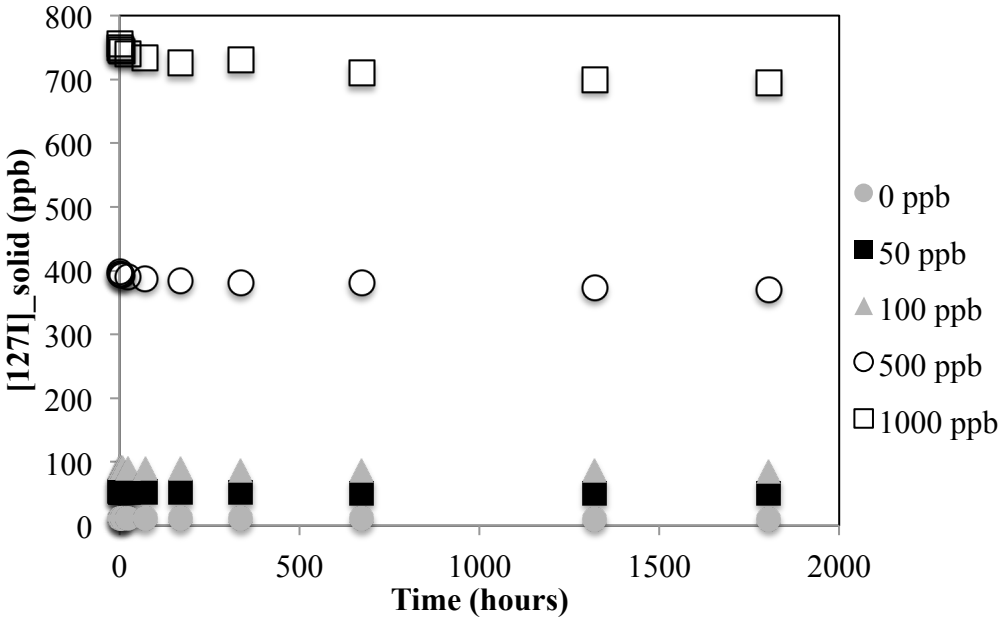


Figure D17. Zero-order model for desorption of iodate (sorbed).

SECOND-ORDER DESORPTION:

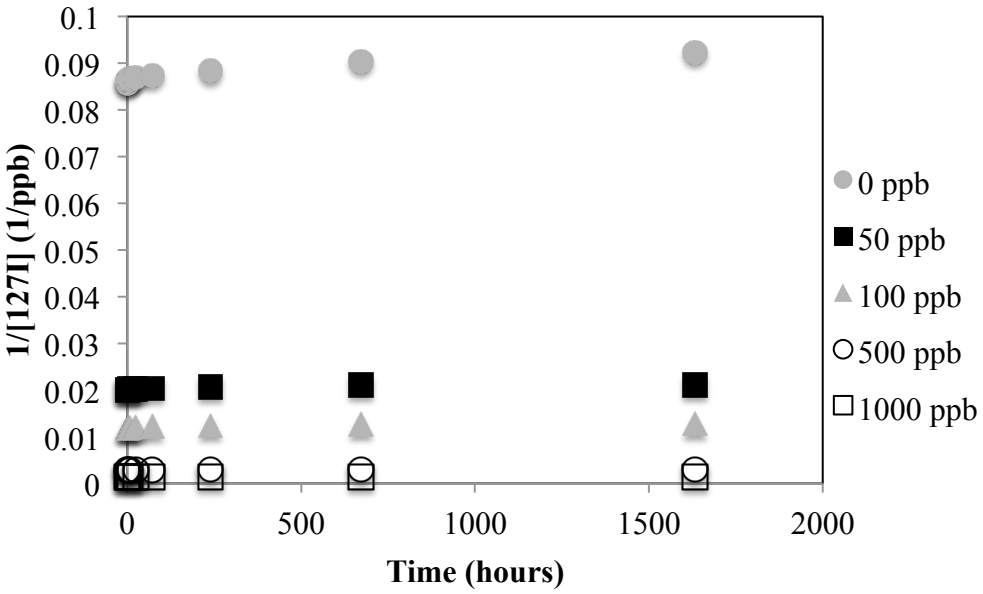


Figure D18. Second-order model for desorption of iodide (sorbed).

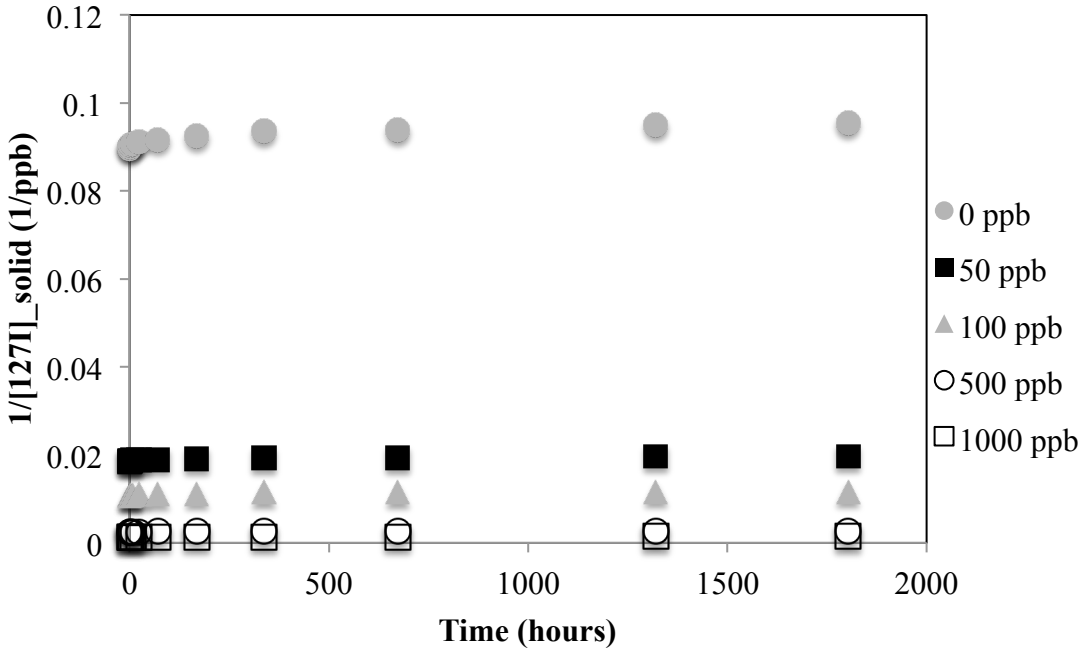


Figure D19. Second-order model for desorption of iodate (sorbed).

APPENDIX E: KINETIC DESORPTION NUMERICAL MODEL

First, Equation 8 was written as variables, yielding Equation E1:

$$z = a * C1^{x} + b * C2^{y} \quad \text{[E1]}$$

where: a = $-k_6$, b = $k_5$,

$$z = \frac{\partial [I - OM]_{aq,t}}{\partial t}$$

$$C1 = [I - OM]_{aq,t}$$

$$C2 = [I - OM]_{sorbed,t}$$

Next Equation E1 was written as a system of equations for each time point (subscripts indicate which time points)

$$\begin{aligned} z_1 &= a * {C1_1}^{x} + b * {C2_1}^{y} \\ z_2 &= a * {C1_2}^{x} + b * {C2_2}^{y} \\ z_3 &= a * {C1_3}^{x} + b * {C2_3}^{y} \\ &\vdots \\ z_8 &= a * {C1_8}^{x} + b * {C2_8}^{y} \end{aligned}$$

This system of equations can be written as a matrix:

$$\begin{bmatrix} z_1 \\ z_2 \\ . \\ . \\ . \\ z_8 \end{bmatrix} = a * \begin{bmatrix} C1_1 \\ C1_2 \\ . \\ . \\ . \\ C1_8 \end{bmatrix}^{x} + b * \begin{bmatrix} C2_1 \\ C2_2 \\ . \\ . \\ . \\ C2_8 \end{bmatrix}^{y} \quad \text{[E2]}$$

Constants x and y are applied into each matrix, yielding Equation E3:

$$\begin{bmatrix} z_1 \\ z_2 \\ . \\ . \\ . \\ z_8 \end{bmatrix} = \begin{bmatrix} a \\ b \end{bmatrix} * \begin{bmatrix} C1_1 & C2_1 \\ C1_2 & C2_2 \\ . & . \\ . & . \\ . & . \\ C1_8 & C2_8 \end{bmatrix} \quad \text{[E3]}$$

Now Equation E3 is rewritten for simplicity, which becomes Equation E4:

$$z = \alpha * C \quad \text{[E4]}$$

Where $\alpha$ is the matrix containing the constants a and b, and C is the matrix containing all of the concentrations:

$$\alpha = \begin{bmatrix} a \\ b \end{bmatrix} \qquad C = \begin{bmatrix} C1_1 & C2_1 \\ C1_2 & C2_2 \\ . & . \\ . & . \\ . & . \\ C1_8 & C2_8 \end{bmatrix}$$

Typically when we take the inverse of C and multiply both sides of the equations by it, because C * $C1^{-1}$ = I (the unit matrix), like so:

$$C^{-1} * z = \alpha * C * C^{-1}$$

However, C was determinant of zero, (i.e. non-singular) and therefore it was impossible to calculate the inverse of C. In order to take the inverse, the matrix has to be a square matrix (i.e. have the same number of rows as is does columns). There are ways to make the matrix square, but it was still non-singular. So instead, Equation E4 was left divided by C on both sides (because C\C = I, as well):

$$z\backslash C = \alpha * C\backslash C$$

Left division worked. And when the equation was solved it was found that a = -1 and b = 0.2427, yielding Equation 12.

APPENDIX F: DATA FROM FIGURES

Table F1. Data from Figure 2

| Percent SRS Wetland Soil of Total Soil (%) | Day 3 $K_d$ (mL/g) | Day 14 $K_d$ (mL/g) | Week 8 $K_d$ (mL/g) |
|---|---|---|---|
| 5 | 2.63 | 3.17 | 4.39 |
| 10 | 2.77 | 4.82 | 6.06 |
| 20 | 3.84 | 6.96 | 9.33 |
| 50 | 4.73 | 9.31 | 20.15 |
| 75 | 4.85 | 11.70 | 22.44 |
| 100 | 1.56 | 10.77 | 19.06 |

Table F2. Data from Figure 3: normalized concentrations over time for each initial spiked concentration of iodide.

| Time (h) | 0 ppb | 50 ppb | 100 ppb | 500 ppb | 1000 ppb |
|---|---|---|---|---|---|
| 1 | 0.54 | 0.92 | 0.95 | 0.94 | 0.96 |
| 3 | 0.39 | 0.87 | 0.91 | 0.94 | 0.94 |
| 8 | 0.33 | 0.76 | 0.81 | 0.87 | 0.88 |
| 24 | 0.29 | 0.57 | 0.64 | 0.72 | 0.73 |
| 72 | 0.22 | 0.43 | 0.46 | 0.46 | 0.46 |
| 240 | 0.16 | 0.38 | 0.40 | 0.36 | 0.32 |
| 336 | 0.16 | 0.36 | 0.40 | 0.39 | 0.34 |
| 672 | 0.16 | 0.32 | 0.36 | 0.36 | 0.32 |
| 1344 | 0.16 | 0.23 | 0.28 | 0.32 | 0.30 |
| 1680 | 0.17 | 0.22 | 0.26 | 0.30 | 0.28 |

Table F3. Data from Figure 4: normalized concentrations over time for each initial spiked concentration of iodate.

| Time (h) | 0 ppb | 50 ppb | 100 ppb | 500 ppb | 1000 ppb |
|---|---|---|---|---|---|
| 1 | 0.82 | 0.80 | 0.82 | 0.82 | 0.83 |
| 3 | 0.77 | 0.76 | 0.76 | 0.77 | 0.77 |
| 8 | 0.65 | 0.63 | 0.62 | 0.64 | 0.67 |
| 24 | 0.49 | 0.46 | 0.46 | 0.49 | 0.54 |
| 76.6667 | 0.36 | 0.36 | 0.36 | 0.38 | 0.43 |
| 170 | 0.31 | 0.31 | 0.31 | 0.34 | 0.37 |
| 337.3333 | 0.28 | 0.27 | 0.28 | 0.31 | 0.34 |
| 674 | 0.25 | 0.23 | 0.26 | 0.28 | 0.31 |
| 1346 | 0.21 | 0.19 | 0.22 | 0.25 | 0.28 |
| 1704.5 | 0.20 | 0.18 | 0.20 | 0.24 | 0.26 |

Table F4. Data from Figure 5: Aqueous iodine concentration over time for 0 ppb of spiked iodide.

| Time (h) | Aqueous Iodine Concentration (ppb) | Standard Deviation (ppb) |
|---|---|---|
| 0 | 0.00 | 0.01 |
| 1 | 0.08 | 0.03 |
| 3 | 0.10 | 0.00 |
| 8 | 0.13 | 0.01 |
| 24 | 0.18 | 0.02 |
| 72 | 0.23 | 0.03 |
| 240 | 0.35 | 0.02 |
| 672 | 0.63 | 0.15 |
| 1632 | 0.84 | 0.43 |

Table F5. Data from Figure 5: Aqueous iodine concentration over time for 50 ppb of spiked iodide.

| Time (h) | Aqueous Iodine Concentration (ppb) | Standard Deviation (ppb) |
|---|---|---|
| 0 | 0.00 | 0.01 |
| 1 | 0.34 | 0.03 |
| 3 | 0.49 | 0.03 |
| 8 | 0.69 | 0.03 |
| 24 | 0.95 | 0.03 |
| 72 | 1.20 | 0.03 |
| 240 | 1.74 | 0.19 |
| 672 | 2.65 | 0.38 |
| 1632 | 2.87 | 0.55 |

Table F6. Data from Figure 5: Aqueous iodine concentration over time for 100 ppb of spiked iodide.

| Time (h) | Aqueous Iodine Concentration (ppb) | Standard Deviation (ppb) |
|---|---|---|
| 0 | 0.00 | 0.11 |
| 1 | 0.81 | 0.10 |
| 3 | 1.10 | 0.30 |
| 8 | 1.61 | 0.55 |
| 24 | 2.34 | 1.14 |
| 72 | 2.89 | 1.32 |
| 240 | 3.65 | 0.80 |
| 672 | 5.29 | 1.24 |
| 1632 | 6.24 | 1.74 |

Table F7. Data from Figure 5: Aqueous iodine concentration over time for 500 ppb of spiked iodide.

| Time (h) | Aqueous Iodine Concentration (ppb) | Standard Deviation (ppb) |
|---|---|---|
| 0 | 0.00 | 0.08 |
| 1 | 3.60 | 0.27 |
| 3 | 4.81 | 0.20 |
| 8 | 6.44 | 0.27 |
| 24 | 8.47 | 0.25 |
| 72 | 11.33 | 0.58 |
| 240 | 16.43 | 0.49 |
| 672 | 24.98 | 0.60 |
| 1632 | 28.18 | 1.38 |

Table F8. Data from Figure 5: Aqueous iodine concentration over time for 1000 ppb of spiked iodide.

| Time (h) | Aqueous Iodine Concentration (ppb) | Standard Deviation (ppb) |
|---|---|---|
| 0 | 0.00 | 1.14 |
| 1 | 5.75 | 0.77 |
| 3 | 8.29 | 0.63 |
| 8 | 11.42 | 0.78 |
| 24 | 16.16 | 0.82 |
| 72 | 21.71 | 0.41 |
| 240 | 32.36 | 0.77 |
| 672 | 51.62 | 1.36 |
| 1632 | 63.38 | 2.52 |

Table F9. Data from Figure 5: Aqueous iodine concentration over time for 0 ppb of spiked iodate.

| Time (h) | Aqueous Iodine Concentration (ppb) | Standard Deviation (ppb) |
|---|---|---|
| 0 | 0.00 | 0.00 |
| 1 | 0.09 | 0.01 |
| 3 | 0.11 | 0.02 |
| 8 | 0.15 | 0.02 |
| 24 | 0.21 | 0.02 |
| 71 | 0.28 | 0.03 |
| 168.25 | 0.38 | 0.02 |
| 336.75 | 0.49 | 0.03 |
| 672 | 0.53 | 0.07 |
| 1320 | 0.66 | 0.09 |
| 1803.5 | 0.71 | 0.11 |

Table F10. Data from Figure 5: Aqueous iodine concentration over time for 50 ppb of spiked iodate.

| Time (h) | Aqueous Iodine Concentration (ppb) | Standard Deviation (ppb) |
|---|---|---|
| 0 | 0.00 | 0.06 |
| 1 | 0.40 | 0.05 |
| 3 | 0.52 | 0.07 |
| 8 | 0.71 | 0.06 |
| 24 | 0.90 | 0.08 |
| 71 | 1.20 | 0.10 |
| 168.25 | 1.67 | 0.12 |
| 336.75 | 2.28 | 0.03 |
| 672 | 2.63 | 0.10 |
| 1320 | 3.16 | 0.16 |
| 1803.5 | 3.28 | 0.15 |

Table F11. Data from Figure 5: Aqueous iodine concentration over time for 100 ppb of spiked iodate.

| Time (h) | Aqueous Iodine Concentration (ppb) | Standard Deviation (ppb) |
|---|---|---|
| 0 | 0.00 | 0.06 |
| 1 | 0.71 | 0.04 |
| 3 | 0.91 | 0.06 |
| 8 | 1.25 | 0.03 |
| 24 | 1.57 | 0.04 |
| 71 | 2.17 | 0.09 |
| 168.25 | 2.92 | 0.15 |
| 336.75 | 5.94 | 2.96 |
| 672 | 5.74 | 1.56 |
| 1320 | 6.27 | 1.02 |
| 1803.5 | 6.49 | 0.84 |

Table F12. Data from Figure 5: Aqueous iodine concentration over time for 500 ppb of spiked iodate.

| Time (h) | Aqueous Iodine Concentration (ppb) | Standard Deviation (ppb) |
|---|---|---|
| 0 | 0.00 | 0.17 |
| 1 | 3.42 | 0.04 |
| 3 | 4.38 | 0.17 |
| 8 | 6.08 | 0.44 |
| 24 | 7.65 | 0.44 |
| 71 | 10.39 | 0.53 |
| 168.25 | 13.95 | 0.63 |
| 336.75 | 18.08 | 1.72 |
| 672 | 17.51 | 7.13 |
| 1320 | 25.14 | 0.61 |
| 1803.5 | 27.53 | 0.61 |

Table F13. Data from Figure 5: Aqueous iodine concentration over time for 1000 ppb of spiked iodate.

| Time (h) | Aqueous Iodine Concentration (ppb) | Standard Deviation (ppb) |
|---|---|---|
| 0 | 0.00 | 0.53 |
| 1 | 6.46 | 1.28 |
| 3 | 8.57 | 1.61 |
| 8 | 12.00 | 1.97 |
| 24 | 15.98 | 2.41 |
| 71 | 22.55 | 3.58 |
| 168.25 | 30.16 | 4.78 |
| 336.75 | 25.27 | 24.98 |
| 672 | 45.99 | 8.29 |
| 1320 | 56.11 | 8.87 |
| 1803.5 | 61.44 | 8.63 |

Table F14. Data from Figure 5: Iodide desorption numerical model data. The iodate numerical model data is similar, but it is not shown in Figure 5 for simplicity.

| Time (hrs) | 0 ppb Model (ppb) | 50 ppb Model (ppb) | 100 ppb Model (ppb) | 500 ppb Model (ppb) | 1000 ppb Model (ppb) |
|---|---|---|---|---|---|
| 1.00 | 0.31 | 0.60 | 1.10 | 3.76 | 5.96 |
| 1.26 | 0.32 | 0.62 | 1.16 | 3.99 | 6.41 |
| 1.58 | 0.33 | 0.65 | 1.22 | 4.25 | 6.89 |
| 2.00 | 0.33 | 0.68 | 1.28 | 4.52 | 7.40 |
| 2.51 | 0.34 | 0.71 | 1.35 | 4.81 | 7.96 |
| 3.16 | 0.35 | 0.74 | 1.42 | 5.12 | 8.56 |
| 3.98 | 0.35 | 0.78 | 1.50 | 5.46 | 9.21 |
| 5.01 | 0.36 | 0.81 | 1.58 | 5.81 | 9.91 |
| 6.31 | 0.37 | 0.85 | 1.67 | 6.19 | 10.66 |
| 7.94 | 0.38 | 0.90 | 1.76 | 6.59 | 11.47 |
| 10.00 | 0.39 | 0.94 | 1.86 | 7.03 | 12.35 |
| 12.59 | 0.40 | 0.99 | 1.97 | 7.49 | 13.29 |
| 15.85 | 0.41 | 1.04 | 2.08 | 7.98 | 14.31 |
| 19.95 | 0.43 | 1.10 | 2.20 | 8.51 | 15.40 |
| 25.12 | 0.44 | 1.16 | 2.33 | 9.07 | 16.59 |
| 31.62 | 0.45 | 1.22 | 2.47 | 9.67 | 17.86 |
| 39.81 | 0.47 | 1.29 | 2.61 | 10.31 | 19.23 |
| 50.12 | 0.49 | 1.37 | 2.77 | 10.99 | 20.71 |
| 63.10 | 0.51 | 1.44 | 2.94 | 11.73 | 22.30 |
| 79.43 | 0.53 | 1.53 | 3.11 | 12.51 | 24.02 |
| 100.00 | 0.55 | 1.62 | 3.30 | 13.34 | 25.88 |
| 125.89 | 0.57 | 1.71 | 3.50 | 14.23 | 27.87 |
| 158.49 | 0.59 | 1.82 | 3.71 | 15.18 | 30.03 |
| 199.53 | 0.62 | 1.93 | 3.94 | 16.20 | 32.35 |
| 251.19 | 0.65 | 2.04 | 4.18 | 17.28 | 34.85 |
| 316.23 | 0.68 | 2.17 | 4.44 | 18.44 | 37.54 |
| 398.11 | 0.71 | 2.30 | 4.71 | 19.68 | 40.45 |
| 501.19 | 0.75 | 2.45 | 5.01 | 21.00 | 43.58 |
| 630.96 | 0.79 | 2.60 | 5.32 | 22.42 | 46.96 |
| 794.33 | 0.83 | 2.76 | 5.65 | 23.92 | 50.60 |
| 1000.00 | 0.87 | 2.94 | 6.00 | 25.54 | 54.52 |
| 1258.93 | 0.92 | 3.13 | 6.38 | 27.26 | 58.75 |
| 1584.89 | 0.97 | 3.33 | 6.78 | 29.09 | 63.30 |
| 1995.26 | 1.02 | 3.55 | 7.21 | 31.06 | 68.22 |

Table F15. Data from Figure 6: Iodine speciation distribution of control samples.

| Control Sample | % I- | % Std Dev | % IO3- | % Std Dev | % OM-I | % Std Dev |
|---|---|---|---|---|---|---|
| Iodide | 97.46 | 0.30 | ---- | ---- | ---- | ---- |
| Iodate | 19.16 | 1.66 | 69.38 | 0.47 | 11.46 | 0.47 |
| 4-iodoaniline | 29.26 | 5.03 | -5.93 | 2.14 | 76.67 | 2.14 |
| L-thyroxine | 29.19 | 27.91 | 26.33 | 6.90 | 44.48 | 6.90 |

Table F16. Data from Figure 7: Iodine speciation from iodate kinetic batch sorption experiment week 10 supernatant.

| Spiked Concentration | % I- | % Std Dev | % IO3- | % Std Dev | % OM-I | % Std Dev |
|---|---|---|---|---|---|---|
| 0 ppb | 9.77 | 3.23 | -29.50 | 67.57 | 119.73 | 65.06 |
| 50 ppb | 6.24 | 3.61 | -0.77 | 36.18 | 94.53 | 32.62 |
| 100 ppb | 3.07 | 1.52 | 14.50 | 19.16 | 82.43 | 17.64 |
| 500 ppb | 6.24 | 2.52 | 62.46 | 18.16 | 31.30 | 15.73 |
| 1000 ppb | 6.49 | 4.25 | 86.78 | 9.45 | 6.73 | 6.58 |

Table F17. Data from Figure 8: Iodine speciation at the end of kinetic desorption experiments where iodide was initially spiked into solution.

| Spiked I- Concentration | % I- | % Std Dev | % IO3- | % Std Dev | % OM-I | % Std Dev |
|---|---|---|---|---|---|---|
| 500 ppb | 29.44 | 11.70 | 10.89 | 11.93 | 59.67 | 10.80 |
| 1000 ppb | 10.44 | 1.47 | 33.68 | 12.26 | 55.88 | 13.46 |

Table F18. Data from Figure 9: Iodine speciation at the end of kinetic desorption experiments where iodate was initially spiked into solution.

| Spiked IO3- Concentration | % I- | % Std Dev | % IO3- | % Std Dev | % OM-I | % Std Dev |
|---|---|---|---|---|---|---|
| 500 ppb | 21.11 | 16.04 | 41.09 | 18.77 | 37.79 | 2.72 |
| 1000 ppb | 40.42 | 0.63 | 34.95 | 3.08 | 24.63 | 2.45 |

Table F19. Data from Figure 10: Iodine speciation of iodate spiked into aqueous organic matter form the SRS wetland soil.

| Spiked Concentration | % I- | % Std Dev | % IO3- | % Std Dev | % OM-I | % Std Dev |
|---|---|---|---|---|---|---|
| Sample 1 | 13.66 | 0.23 | 736.78 | 81.97 | 0.01 | 4.37 |
| Sample 2 | 4.17 | 0.12 | 734.42 | 89.96 | 0.08 | 5.87 |
| Sample 3 | 10.11 | 0.41 | 724.79 | 86.18 | 0.02 | 3.71 |
| Sample 4 | 20.26 | 0.41 | 770.16 | 77.28 | 0.01 | 2.47 |

APPENDIX G: ORGANOIODINE CONCENTRATIONS AT END OF IODATE KINETIC BATCH SORPTION EXPERIMENT

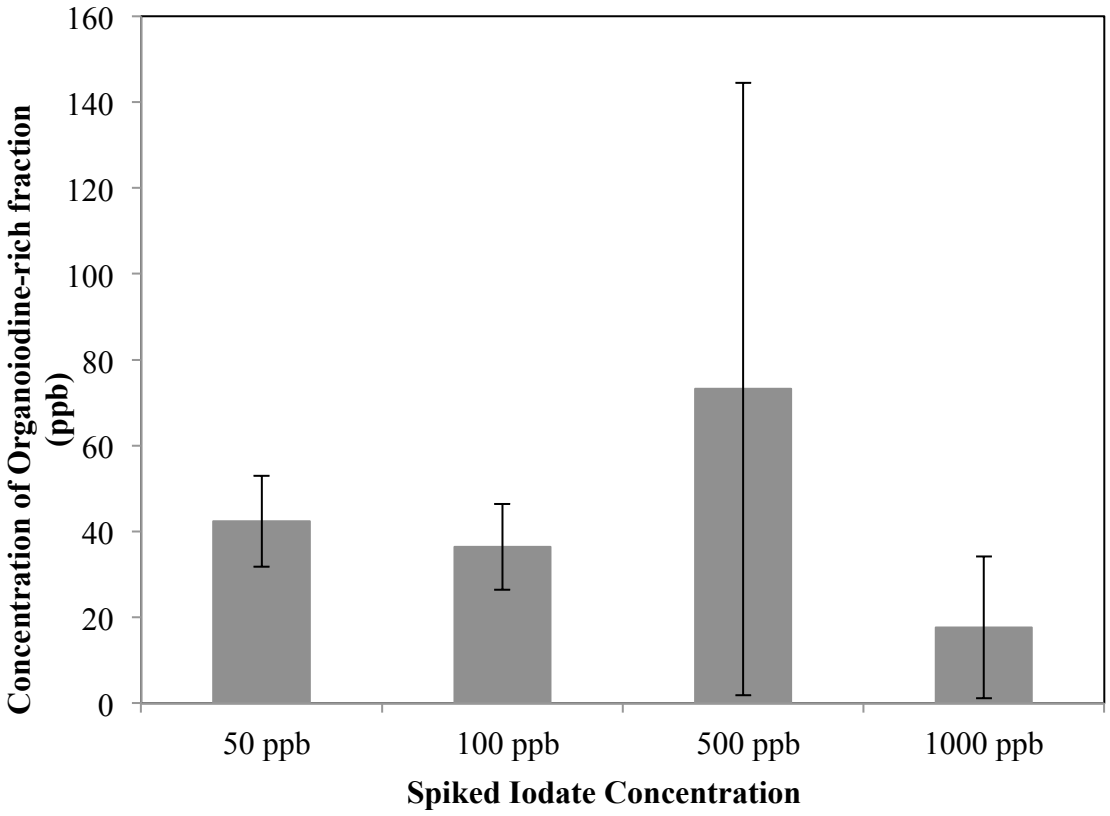


Figure G1. Concentration of iodine organoiodine-rich fraction when iodate was spiked into dissolved organic carbon from the SRS wetland sediments. Concentrations are similar across all initially spiked iodate concentrations.

# APPENDIX H: ACS COPYRIGHT FROM FIGURE 1



Copyright Clearance Center RightsLink®

Home | Create Account | Help

ACS Publications
Most Trusted. Most Cited. Most Read.

**Title:** Evaluation of a Radioiodine Plume Increasing in Concentration at the Savannah River Site

**Author:** Daniel I. Kaplan, Kimberly A. Roberts, Kathy A. Schwehr, et al

**Publication:** Environmental Science & Technology

**Publisher:** American Chemical Society

**Date:** Jan 1, 2011



LOGIN

**If you're a copyright.com user,** you can login to RightsLink using your copyright.com credentials. Already **a RightsLink user** or want to learn more?

**PERMISSION/LICENSE IS GRANTED FOR YOUR ORDER AT NO CHARGE**

This type of permission/license, instead of the standard Terms & Conditions, is sent to you because no fee is being charged for your order. Please note the following:

- Permission is granted for your request in both print and electronic formats, and translations.
- If figures and/or tables were requested, they may be adapted or used in part.
- Please print this page for your records and send a copy of it to your publisher/graduate school.
- Appropriate credit for the requested material should be given as follows: "Reprinted (adapted) with permission from (COMPLETE REFERENCE CITATION). Copyright (YEAR) American Chemical Society." Insert appropriate information in place of the capitalized words.
- One-time permission is granted only for the use specified in your request. No additional uses are granted (such as derivative works or other editions). For any other uses, please submit a new request.

If credit is given to another source for the material you requested, permission must be obtained from that source.

BACK | CLOSE WINDOW

8. REFERENCES

Amachi, S.; Fujii, T.; Shinoyama, H.; Muramatsu, Y. Microbial Influences on the Mobility and Transformation of Radioactive Iodine in the Environment. J. Nucl. and Radiochem. Sci, 2005, 6-1, 21–24.

Álvarez, F., Reich, M., Snyder, G., Pérez-Fodich, A., Muramatsu, Y., Daniele, L., & Fehn, U. (2016). Iodine budget in surface waters from Atacama: Natural and anthropogenic iodine sources revealed by halogen geochemistry and iodine-129 isotopes. *Applied Geochemistry, 68*, 53-63. doi:10.1016/j.apgeochem.2016.03.011

Barber, K. (2017). *Evaluation of Aging Process Controlling Cesium Transport through Savannah River Site Soils* (Unpublished master's thesis). Clemson University.

Bowley, H., Young, S., Ander, E., Crout, N., Watts, M., & Bailey, E. (2016). Iodine binding to humic acid. *Chemosphere, 157*, 208-214. doi:10.1016/j.chemosphere.2016.05.028

Chang, H., Xu, C., Schwehr, K. A., Zhang, S., Kaplan, D. I., Seaman, J. C., . . . Santschi, P. H. (2014). Model of radioiodine speciation and partitioning in organic-rich and organic-poor soils from the Savannah River Site. Journal of Environmental Chemical Engineering, 2(3), 1321-1330. doi:10.1016/j.jece.2014.03.009 .

Davis, K., Vidmar, M., Khasanov, A., Cole, B., Ghelardini, M., Mayer, J., . . . Mefford, O. T. (2018). The effect of post-synthesis aging on the ligand exchange activity of iron oxide nanoparticles. *Journal of Colloid and Interface Science, 511*, 374-382. doi:10.1016/j.jcis.2017.09.087

Denham, M.; Vangelas, K. M., Biogeochemical gradients as a framework for understanding waste-site evolution. Remediation 2008, Winter 2008, 5−17.

Emerson, H. P., Xu, C., Ho, Y., Zhang, S., Schwehr, K. A., Lilley, M., . . . Powell, B. A. (2014). Geochemical controls of iodine uptake and transport in Savannah River Site subsurface sediments. Applied Geochemistry, 45, 105-113. doi:10.1016/j.apgeochem.2014.03.002.

Federal Register. 2000, 65, 236, December 2.

Fox, P. M., Davis, J. A., & Luther, G. W. (2009). The kinetics of iodide oxidation by the manganese oxide mineral birnessite. *Geochimica et Cosmochimica Acta, 73*(10), 2850-2861. doi:10.1016/j.gca.2009.02.016.

Grogan, K. P., & DeVol, T. A. (2013). Development of a Novel Method for the Determination of Aqueous Inorganic 129I Speciation. *Analytical Chemistry, 85*(9), 4658-4665. doi:10.1021/ac4003084

Hoogsteen, M. J., Lantinga, E. A., Bakker, E. J., Groot, J. C., & Tittonell, P. A. (2015). Estimating soil organic carbon through loss on ignition: effects of ignition conditions and structural water loss. *European Journal of Soil Science, 66*(2), 320-328. doi:10.1111/ejss.12224

Hou, X.; Hansen, V.; Aldahan, A.; Possnert, G.; Lind, O. C.; Lujaniene, G. A review on speciation of iodine-129 in the environment and biological samples. Anal. Chim. Acta 2009, 632, 181–196.

Hu, Q., Zhao, P., Moran, J. E., & Seaman, J. C. (2005). Sorption and transport of iodine species in sediments from the Savannah River and Hanford Sites. *Journal of Contaminant Hydrology, 78*(3), 185-205. doi:10.1016/j.jconhyd.2005.05.007 .

Huber, R. E.; Edwards, L. A.; Carne, T. J. Studies on the mechanism of iodination of tyrosine by lactoperoxidase. J. Biol. Chem. 1989, 264, 1381–1386.

International Atomic Energy Agency, Nuclear Data Section. (2017). Live Chart of the Nuclides. Retrieved November 06, 2017, from https://www-nds.iaea.org/relnsd/vcharthtml/VChartHTML.html

Kahn, M.; Kleinberg, J. Radiochemistry of iodine; National Academy of Sciences−National Research Council. Energy Research and Development Administration, 1977; NAS-NS-3062.

Kaplan, D. I., Roberts, K. A., Schwehr, K. A., Lilley, M. S., Brinkmeyer, R., Denham, M. E., . . . Santschi, P. H. (2011). Evaluation of a Radioiodine Plume Increasing in Concentration at the Savannah River Site. *Environmental Science & Technology, 45*(2), 489-495. doi:10.1021/es103314n MICDS 2012.

Kaplan, D. I., Zhang, S., Roberts, K. A., Schwehr, K., Xu, C., Creeley, D., . . . Santschi, P. H. (2014). Radioiodine concentrated in a wetland. *Journal of Environmental Radioactivity, 131*, 57-61. doi:10.1016/j.jenvrad.2013.09.001

Kaplan, D. I.; Serne, R. J.; Parker, K. E.; Kutnyakov, I.V. Iodide sorption to subsurface sediments and illite minerals. Environ. Sci. Technol. 2000, 34, 399–405.

Li, H.P, Brinkmeyer, R., Jones, W.L., Zhang, S., Xu, C., Ho, Y.F., K.A. Schwehr, K.A., D.I. Kaplan, D.I., P.H. Santschi, P.H, C.M. Yeager, C.MIodide oxidizing activity of bacteria from subsurface sediments of the Savannah River site. K.M.M. Kawaguchi, H. Sato, T. Yokokawa, T. Itai, T.M. Nguyen, J. Ono, S. Tanabe (Eds.), Interdisciplinary Studies on Environmental Chemistry, Environmental Pollution and Ecotoxicology, vol. 6, Terra Scientific Publishing Company, Tokyo (2012), pp. 89-97

Li, J., Wang, Y., Xie, X., Zhang, L., & Guo, W. (2013). Hydrogeochemistry of high iodine groundwater: a case study at the Datong Basin, northern China. Environmental Science: Processes & Impacts, 15(4), 848. doi:10.1039/c3em30841c

Looney, B. B.; Grant, M. W.; King, C. M. Estimation of Geochemical Parameters for Assessing Subsurface Transport at the Savannah River Site, DPST-85-904; E.I. Du Pont de Nemours & Co.: Wilmington, DE, 1987.

Miller, J.N.: Using the Grubbs and Cochran tests to identify outliers. Anal. Methods Commun. **7**, 7948–7950 (2015)

Otosaka, S., Schwehr, K. A., Kaplan, D. I., Roberts, D. A., Zhang, S., Xu, C., Li, H.-P., Ho, Y.-F., Brinkmeyer, R., Yeager, C. M., and Santschi, P. H. (2011). Factors controlling mobility of 127I and 129I species in an acidic groundwater plume at the Savannah River Site. The Science of the Total Environment 409, 3857-3865.

Pommier, J.; Sokoloff, L.; Nunez, J. Enzymatic iodination of protein. Kinetics of Iodine Formation and Protein Iodination Catalyzed by Horse-Radish Peroxidase. Eur. J. Biochem. 2005, 38, 497–506.

Reddy, K. R., & DeLaune, R. D. (2008). *Biogeochemistry of Wetlands : Science and* Applications. Boca Raton: CRC Press.

Rumble, John R. ed., CRC Handbook of Chemistry and Physics, 98th Edition (Internet Version 2018), CRC Press/Taylor & Francis, Boca Raton, FL.

Schwehr, K. A.; Santschi, P. H. Sensitive determination of iodine species, including organo-iodine, for freshwater and seawater samples using high performance liquid chromatography and spectrophotometric detection. Anal. Chim. Acta 2003, 482, 59–71.

Schwehr, K.A., Santschi, P.H., Kaplan, D.I., Yeager, C.M., Brinkmeyer, R., 2009. Organo-iodine formation in soils and aquifer sediments at ambient concentrations. Environ. Sci. Technol. 43, 7258e7264.

Sparks, D.L, Page, A.L., Helmke, P.A., Loeppert, R.H., editors, 1996. Methods of Soil Analysis Part 3—Chemical Methods. SSSA Book Ser. 5.3. SSSA, ASA, Madison, WI. doi:10.2136/sssabookser5.3

SRNS. Annual Corrective Action Report for the F-area Hazardous Waste Management Facility, the H-area Hazardous Waste Management Facility, and the Mixed Waste Management Facility; Savannah River Nuclear Solutions: Aiken, SC, 2010.

Suresh Kumar Reddy, K.; Narender, N.; Rohitha, C. N.; Kulkarni, S. J. Iodination of aromatic compounds using potassium iodide and hydrogen peroxide. Synth. Commun. 2008, 38, 3894–3902.

Wan, J., Tokunaga, T. K., Dong, W., Denham, M. E., & Hubbard, S. S. (2012). Persistent Source Influences on the Trailing Edge of a Groundwater Plume, and Natural Attenuation Timeframes: The F-area Savannah River Site. Environmental Science & Technology, 46(8), 4490-4497. doi:10.1021/es204265q

Warner, J. A.; Casey, W. H.; Dahlgren, R. A. Interaction kinetics of I2(aq) with substituted phenols and humic substances. Environ. Sci. Technol. 2000, 34, 3180–3185.

Xu, C., Zhong, J.Y., Hatcher, P.G., Zhang, S., Li, H.-P., Ho, Y.-F., Schwehr, K.A., Kaplan, D.I., Roberts, K.A., Brinkmeyer, R., Yeager, C.M., Santschi, P.H., 2012. The molecular environment of stable iodine and radioiodine (129I) in natural organic matter: evidence from NMR. Geochim. Cosmochim. Acta 97, 166–182.

Xu, C., Chen, H., Sugiyama, Y., Zhang, S., Li, H., Ho, Y., . . . Santschi, P. H. (2013). Novel molecular-level evidence of iodine binding to natural organic matter from Fourier transform ion cyclotron resonance mass spectrometry. *Science of The Total Environment, 449*, 244-252. doi:10.1016/j.scitotenv.2013.01.064

Zhang, S.; Du, J.; Xu, C.; Schwehr, K. A.; Ho, Y. F.; Li, H. P.; Roberts, K. A.; Kaplan, D. I.; Brinkmeyer, R.; Yeager, C. M.; Chang, H. S.; Santschi, P. H. Concentration-dependent mobility, retardation, and speciation of iodine in surface sediment from the Savannah River site. Environ. Sci. Technol. 2011, 45 (13), 5543−5549.